공학석사학위논문

Structural Design and Analysis of All-moving Type Smart Fin using Single-crystal Piezoelectric Actuator

단결정 압전재료 작동기를 이용한 강체 회전형태의 지능형 조종익 구조 설계 및 해석

2017년 2월

서울대학교 대학원

기계항공공학부

박 철 우

Structural Design and Analysis of All-moving Type Smart Fin using Single-crystal Piezoelectric Actuator

단결정 압전재료 작동기를 이용한 강체 회전형태의 지능형 조종익 구조 설계 및 해석

지도교수 신상준

이 논문을 공학석사 학위논문으로 제출함

2017년 2월

서울대학교 대학원

기계항공공학부

박 철 우

박철우의 석사학위논문을 인준함

2017년 2월

위 원 장 _____ (인)

부 위 원 장 _____ (인)

위 원 _____ (인)

Abstract

Structural Design and Analysis of All-moving Type Smart Fin using Single-crystal Piezoelectric Actuator

Chul woo Park

Mechanical and Aerospace Engineering

The Graduate School

Seoul National University

Researches regarding piezoelectric actuators has been conducted to substitute for the hydraulic actuators by the piezoelectric material because of light weight and accurate actuation. In this thesis, an actuating mechanism of the smart fin using single-crystal piezoelectric actuator is developed and structural analysis regarding the resulting pitch rotation angle is conducted. A straight unimorph actuator is embedded along the spanwise direction inside the hollow inner space of the airfoil. A hinge which is constrained about its axial rotation is located at 1/4 of chord, and thus the smart fin rotates in its rigid pitch direction. Structural behavior of the smart fin was predicted by using commercial software program ANSYS, regarding the resulting actuation of the trailing edge under specific voltage input in the air. In addition, the flutter analysis was conducted on the structure to confirm the stability condition under Mach number 0.5 flight.

Keywords: Smart Fin, Piezoelectric Material, Smart Structure Theory, ANSYS Structural Analysis, ANSYS FLUENT, Aeroelasticity, Flutter, ZAERO, Modal Analysis

Student Number: 2015-20771

Table of Contents

List of Figures

List of Tables

I. Introduction

1.1 Backgrounds and Motivation

Development of composite material has progressed in the field of aerospace engineering. Those advancement are called smart structures. Smart structures consist of sensors and actuators which are attached or embedded in the existing structures. Via a sensor and actuator network, it can respond to external environment or specific operational requirements [1]. Recently, several researches regarding the actuators using piezoelectric material has been conducted because of its light weight and accurate actuation. Yoon [2] developed an actuator including single-crystal piezoelectric material, called PMN-29PT. The actuator using PMN-29PT shows 1.6 times larger strain than those of the other lightweight piezoelectric actuator (LIPCA) using CTS 3203HD. CTS 3203HD is a poly-crystal piezoelectric material and PMN-29PT has improved dielectric constant (d_{31}) than CTS 3203HD does.

Substituting for the hydraulic actuator by the piezoelectric material was

attempted because high performance of piezoelectric material was developed. Therefore, analysis of smart structure using piezoelectric material was conducted by several researchers. Researches on the smart fin design concept was conducted by Rabinovitch [3]. The feasibility of using monolithic, directed, or fibrous piezoelectric materials was examined to control the shape of a subsonic projectile fin during flight. An analytical model for composite laminated plates of general layup with either isotropic or anisotropic active layers was derived. The mathematical formulation used the principle of virtual work along with the classical plate and lamination theories and the anisotropic piezoelectric constitutive equations. Through those equations, four basic design concepts for twist actuation and shape control of the smart fin was developed as shown in Fig 1.4. And the performance of those fins was compared by using finite element analysis. Another research on the smart fin was conducted by Barret [4]. Barret conducted research about a fin including a torque plate composed of piezoelectric material as shown in Fig 1.5. The tip of the plate was bonded to an aerodynamic shell which undergoes a pitch change as the plate twists. The torque plate produced the static twist deflection of $\pm 3°$. The NACA0012 aerodynamic shell, mounted in wind tunnel at speed up to 50m/s, showed the pitch deflection of $\pm 2°$ at air speed of 40m/s.

The researches regarding stability aspects of the control fin were also conducted by several researchers. Research about free/forced vibration suppression of the smart fin was performed by Sahin [5]. Sixteen piezoelectric plates were used to change the shape of the smart fin. H-infinity controller and μ-synthesis controller were designed to stabilize the system of the smart fin. In analysis, ANSYS and MATLAB were used for modeling the structures and observing time and frequency response, respectively.

1.2 Objectives and Thesis Overview

In this thesis, various concepts of the smart fin using piezoelectric actuator are designed. Performance of the smart fin should satisfy the maximum pitch rotation angle of $\pm 10°$. Structural analysis of those concepts is conducted for performance improvement. All concepts of the smart fin are evaluated regarding the all-moving type in which rigid body rotation is induced in pitch direction when the piezoelectric actuator generates bending moment under specific voltage input.

The structural behavior of the smart fin is analyzed using ANSYS Structural analysis to verify the performance of its pitch rotation angle of the airfoil and compared with the experimental results in vacuum. The performance of its pitch rotation angle with aerodynamic load is predicted using ANSYS FLUENT. The aerodynamic hinge moment of the smart fin is predicted to evaluate the aerodynamic effect of the smart fin. By deriving the moment-rotation angle diagram of the smart fin, the resulting rotation angle of smart fin is predicted under Mach number 0.1 flight.

Aeroelastic analysis is also conducted to verify the stability of the smart fin using ZAERO. Mode shapes of the smart fin are predicted using MSC.NASTRAN, and by using those results of modal analysis, flutter speed of the smart fin is predicted to verify stability of the smart fin under Mach number 0.5 flight.

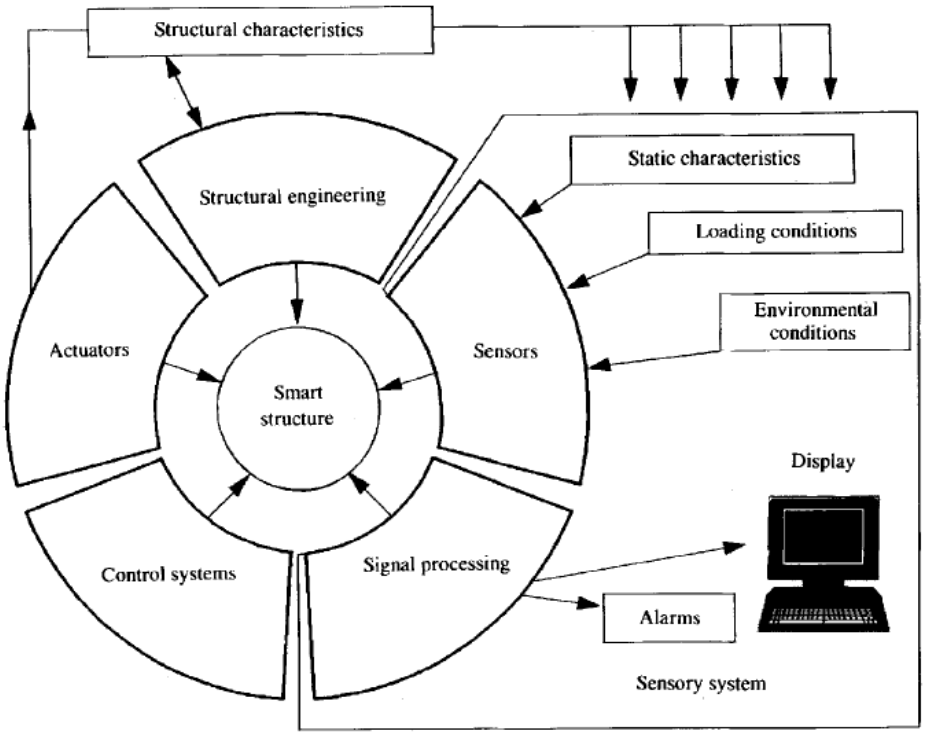

Figure 1.1 Smart Structure: Functional Summary [1]

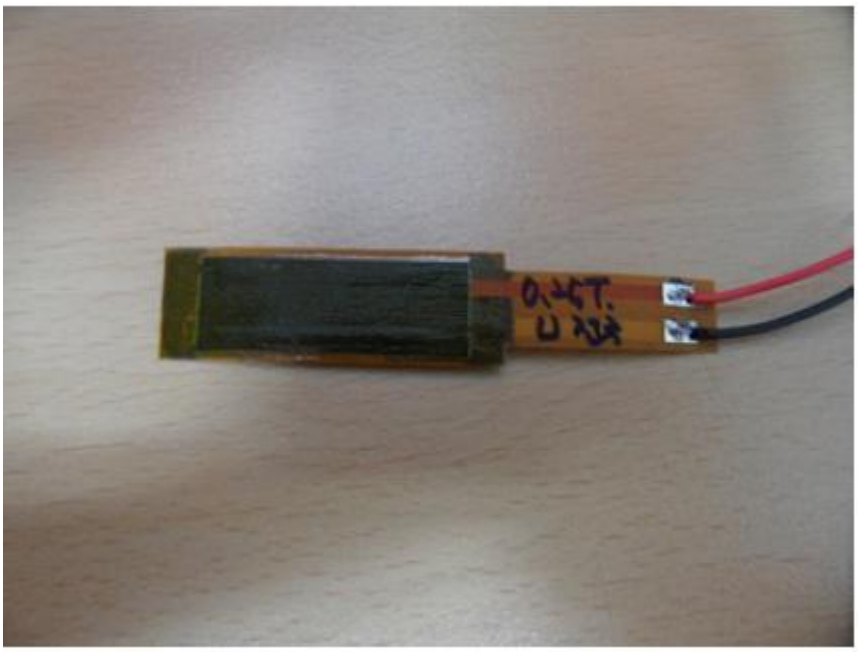

Figure 1.2 Example of S-LIPCA (PMN-29PT) [2]

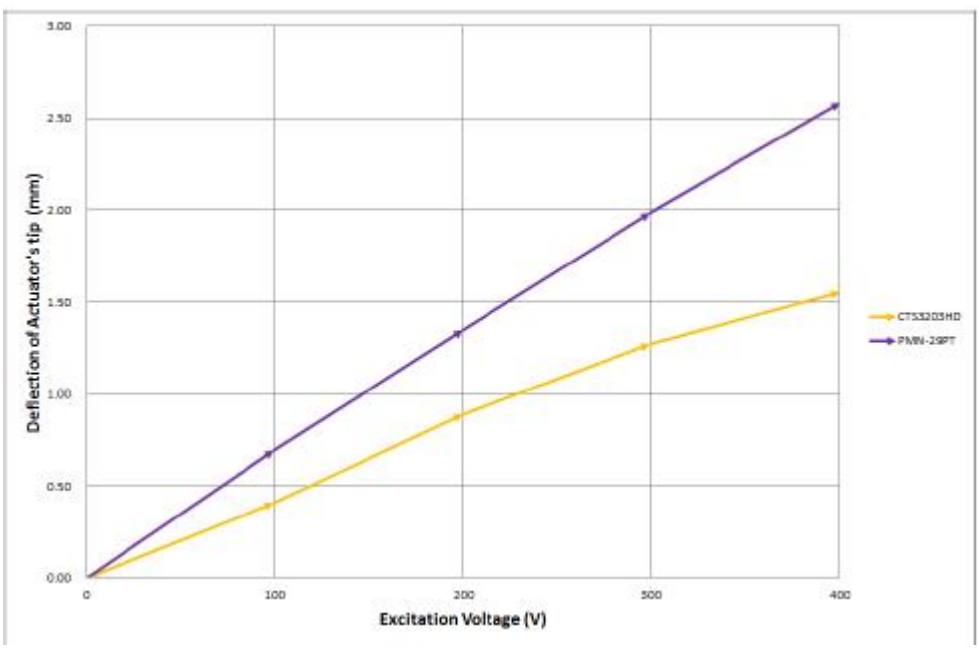

Figure 1.3 Performance of Piezoelectric Actuators [2]

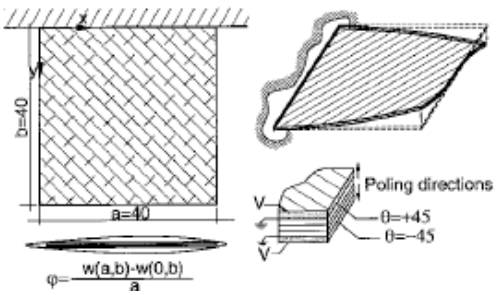

(a) Twist actuation of a cantilevered fin

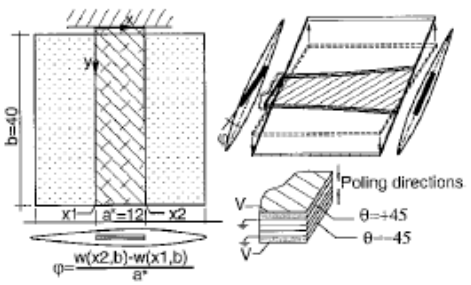

(b) Twist actuation of a central shaft

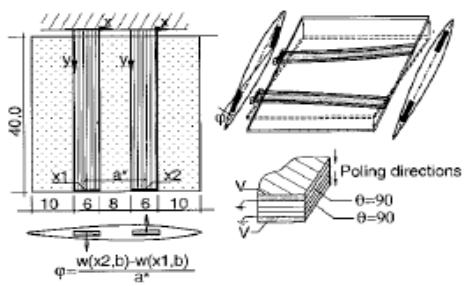

(c) Antı-symmetrıc bendıng ın parallel conﬁguration

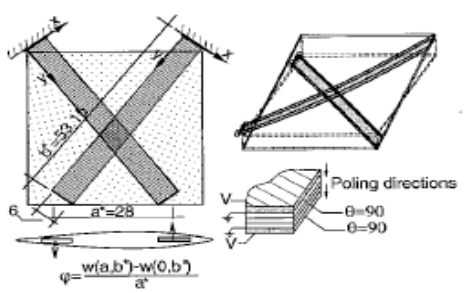

(d) Anti-symmetric bending in diagonal configuration

Figure 1.4 Designs Investigated for the Active Fin [3]

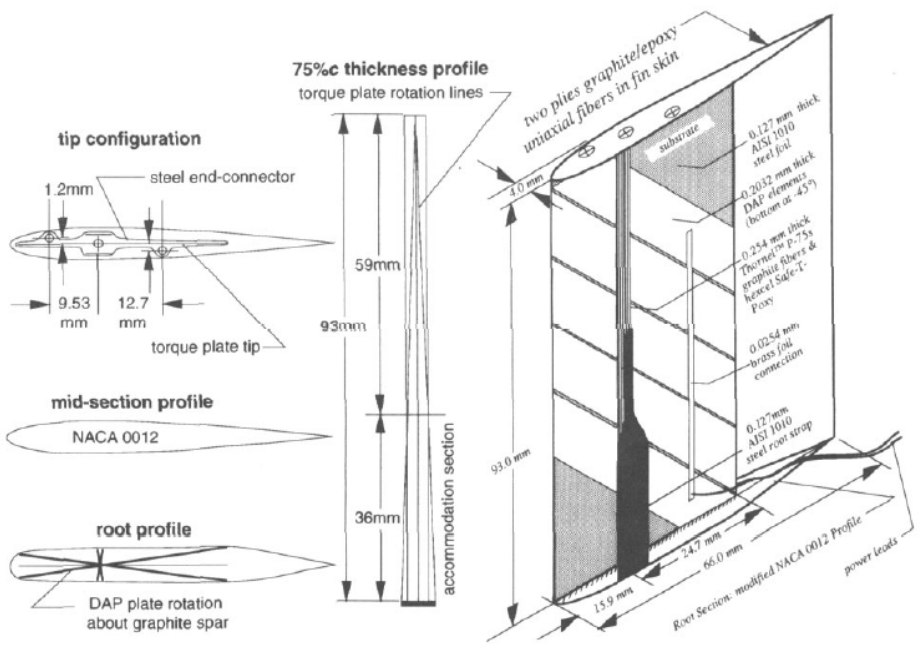

Figure 1.5 DAP Torque Plate and Fin Geometry [4]

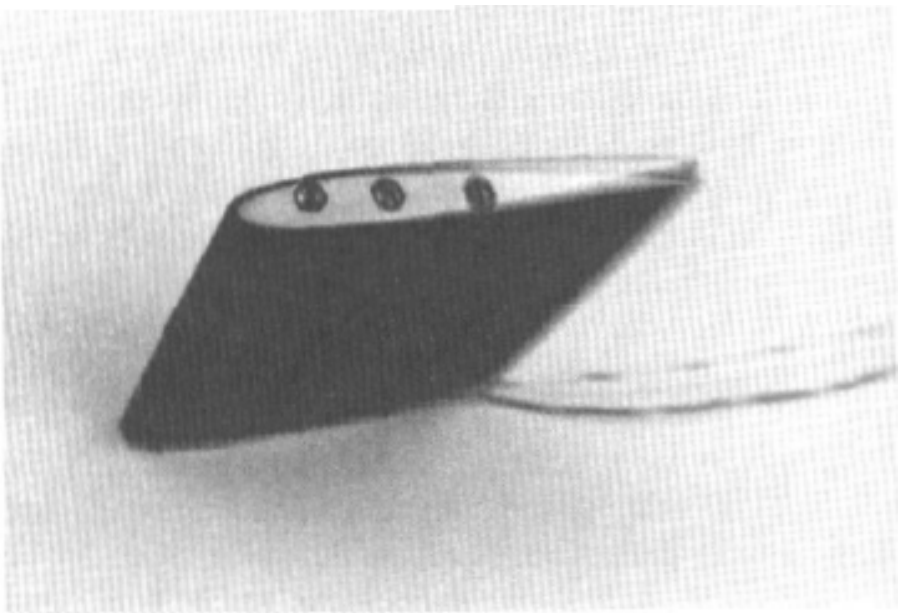

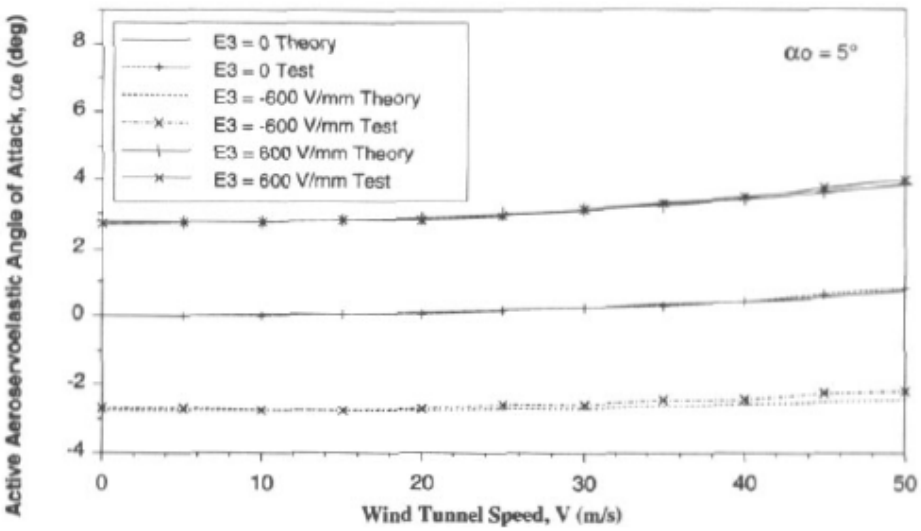

Figure 1.6 Wind Tunnel Test of DAP torque fin [4]

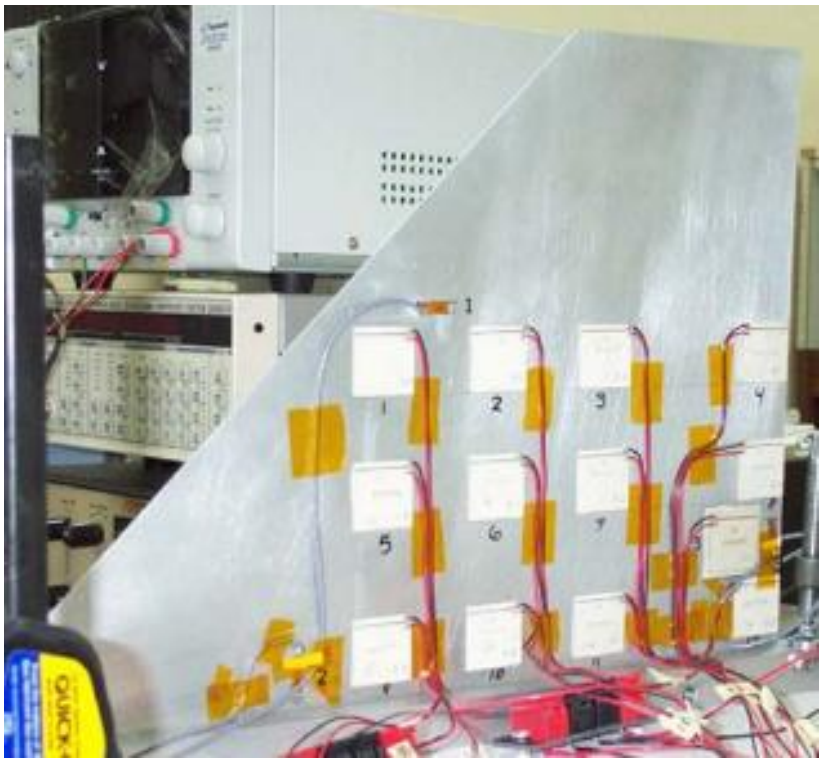

Figure 1.7 Experimental construction of a Smart Fin Controlled by Piezoelectric Plates [5]

II. Theoretical Background

2.1 Stress Form of the Piezoelectric Matrix

For structural analysis using ANSYS, stress form of the piezoelectric matrix is needed. Given the strain form of the piezoelectric equations, it can be converted to the stress form and give expression for the three independent e tensor parameters. It can be expressed in the following matrix form [6].

$$\varepsilon = d^T E + c^{-1}\sigma \tag{1}$$

$$P = \epsilon_0 \chi E + d\sigma \tag{2}$$

where ε is strain tensor, P is the electric polarization vector, E is the electric field vector, σ is the stress tensor, d is the components of the piezoelectric tensor, c is the components of the inverse elastic tensor, χ is the components of the electric susceptibility tensor, and ϵ_0 is the permittivity of the free space.

Multiplying Eqn. (1) by the elasticity matrix,

$$c\varepsilon = cd^T E + \sigma \tag{3}$$

so that it can be solved for the stress matrix σ.

$$\sigma = c\varepsilon - eE \tag{4}$$

where $e = cd^T$. And from Eqn. (2)

$$\begin{aligned} D = P + \epsilon_0 E &= \epsilon_0 \chi E + d\sigma + \epsilon_0 E \\ &= \epsilon_0(\chi + I)E + d\sigma \\ &= \epsilon^\sigma E + d\sigma \end{aligned} \tag{5}$$

where D is the electric displacement vector and ϵ^σ is the permittivity at a constant stress. Substituting the expression for the stress tensor σ which is solved from above

$$\begin{aligned} D &= \epsilon^\sigma E + d(c\varepsilon - eE) \\ &= (\epsilon^\sigma - de)E + dc\varepsilon \\ &= \epsilon^\varepsilon E + e^T \varepsilon \end{aligned} \tag{6}$$

where $\epsilon^\varepsilon = \epsilon^\sigma - de$ is the permittivity at a constant strain. The elastic matrix c has 6 independent parameters and d has three independent parameters as follows [7].

$$c = \begin{bmatrix} c_{11} & c_{12} & c_{13} & 0 & 0 & 0 \\ c_{12} & c_{22} & c_{13} & 0 & 0 & 0 \\ c_{13} & c_{13} & c_{33} & 0 & 0 & 0 \\ 0 & 0 & 0 & c_{44} & 0 & 0 \\ 0 & 0 & 0 & 0 & c_{44} & 0 \\ 0 & 0 & 0 & 0 & 0 & 2(c_{11}-c_{12}) \end{bmatrix} \tag{7}$$

and

$$d = \begin{bmatrix} 0 & 0 & 0 & 0 & d_{15} & 0 \\ 0 & 0 & 0 & d_{15} & 0 & 0 \\ d_{31} & d_{31} & d_{33} & 0 & 0 & 0 \end{bmatrix} \tag{8}$$

Then the piezoelectric stress matrix is described as follows [8].

$$e = cd^T = \begin{bmatrix} c_{11} & c_{12} & c_{13} & 0 & 0 & 0 \\ c_{12} & c_{22} & c_{13} & 0 & 0 & 0 \\ c_{13} & c_{13} & c_{33} & 0 & 0 & 0 \\ 0 & 0 & 0 & c_{44} & 0 & 0 \\ 0 & 0 & 0 & 0 & c_{44} & 0 \\ 0 & 0 & 0 & 0 & 0 & 2(c_{11}-c_{12}) \end{bmatrix} \begin{bmatrix} 0 & 0 & d_{31} \\ 0 & 0 & d_{31} \\ 0 & 0 & d_{33} \\ 0 & d_{15} & 0 \\ d_{15} & 0 & 0 \\ 0 & 0 & 0 \end{bmatrix}$$

$$= \begin{bmatrix} 0 & 0 & c_{11}d_{31}+c_{12}d_{31}+c_{13}d_{33} \\ 0 & 0 & c_{12}d_{31}+c_{11}d_{31}+c_{13}d_{33} \\ 0 & 0 & c_{13}d_{31}+c_{13}d_{31}+c_{33}d_{33} \\ 0 & c_{44}d_{15} & 0 \\ c_{44}d_{15} & 0 & 0 \\ 0 & 0 & 0 \end{bmatrix} \tag{9}$$

2.2 Simple Blocked Force Beam Model: A Symmetric Actuation of

Single Actuator

The blocked force method is a simple and physically intuitive approach to estimate the structural response due to induced strain actuation. Consider a single piezo actuator surface-mounted on the bottom of a cantilevered beam, as shown in Fig. 2.1. In this case, electric voltage applied to the piezo actuator will induce both bending and extension of the beam.

The induced actuator bending-extension relations are derived as follows.

$$\sigma_b - \sigma_b^o = -\frac{M_z}{I_b}(\sigma_b^o : the\ axial\ stress\ at\ the\ neutral\ axis) \tag{10}$$

It can be assumed that the neutral axis is at the mid-plane of the beam because the thickness of the piezo actuators is small compared to that of the beam. The top-surface strain ε_b^s and neutral axis strain ε_b^o are related to the bending moment as follows:

$$\varepsilon_b^s - \varepsilon_b^o = -\frac{M t_b}{2 l_b}\frac{1}{E_b}\ (M = F\frac{t_b}{2}) \tag{11}$$

The bottom surface strain, ε_b^{-s} and mid-plane strain are given by:

$$\varepsilon_b^s - \varepsilon_b^o = \frac{M t_b}{2 l_b}\frac{1}{E_b},\ \varepsilon_b^o = \frac{F}{b_b t_b E_b} = \frac{F}{E_b A_b} \tag{12}$$

Note that in this configuration,

Extensional stiffness of the beam $EA_b = E_b b_b t_b$

Extensional stiffness of the actuator $EA_{c1} = E_c b_c t_c$

Bending stiffness of the beam $EI_b = E_b b_b \frac{t_b^3}{12} = EA_b \frac{t_b^2}{12}$

Bending stiffness of the actuator $EI_{c1} = E_c b_c \frac{t_b^3}{12} + E_c b_c t_c \left(\frac{t_c}{2} + \frac{t_b}{2}\right)^2 \cong EA_{c1}\frac{t_b^2}{4}$

On the bottom surface (at the piezo location),

$$\text{弯矩} = \frac{F\left(\frac{t_b}{2}\right)^2}{b_b \frac{t_b^2}{12}} \frac{1}{E_b} + \frac{F}{EA_b} = \frac{4F}{EA_b}, \Delta l_b^{-s} = \frac{4F}{EA_b}, \Delta l_c = \left(\Lambda - \frac{F}{EA_{c1}}\right) l_c \quad (\text{ max} = d_{31}\frac{V}{t_c} = \Lambda) \tag{13}$$

Displacement compatibility yields $\Delta l_b^{-s} = \Delta l_c$

$$\frac{4F}{EA_b} = \frac{d_{31}V}{t_c} - \frac{F}{EA_{c1}} \tag{14}$$

$$F = \Lambda \frac{EA_b EA_{c1}}{4EA_{c1} + EA_b} = F_{bl} \frac{EA_b}{4EA_{c1} + EA_b} = F_{bl} \frac{3EI_b}{4EI_{c1} + 3EI_b} \tag{15}$$

where the blocked force $F_{bl} = E_c A_c \Lambda = EA_{c1}\Lambda$ $(\Lambda = d_{31}V / t_c)$. This leads to [9]

$$M = M_{bl} \frac{3EI_b}{3EI_b + 4EI_c} \quad (M_{bl} = F_{bl}\frac{t_b}{2}) \tag{16}$$

2.3 Analysis Theories used in ANSYS Structural

In this thesis, ANSYS static and transient structural analysis is used to analyze the actuation of piezoelectric actuator and pitch rotation angle of smart fin. For linear static structural analysis, the displacements $\{x\}$ are solved for in the matrix equation below: [10]

$$[K]\{x\} = \{F\} \tag{17}$$

In linear static analysis, it is assumed that stiffness matrix $[K]$ is constant so that linear elastic material behavior may be assumed. Small deflection theory is used and some nonlinear boundary conditions may be included. $\{F\}$ is statically applied so that no time-varying force may be considered and no inertial effects are included.

In nonlinear analysis, ANSYS uses the Newton-Raphson algorithm. Nonlinear analysis applies the load gradually, in increments, and also performs equilibrium iterations at each load increment to drive the incremental solution to equilibrium.

The matrix equation is expressed below: [11]

$$[K_T]\{\Delta u\} = \{F\} - \{F^{nr}\} \tag{18}$$

where $[K_T]$ is tangent stiffness matrix, $\{\Delta u\}$ is displacement increment, $\{F\}$ is external load vector and $\{F^{nr}\}$ is internal force vector. Iterations will be repeated until $\{F\} - \{F^{nr}\}$ (difference between external and internal loads) is within a tolerance as shown in Fig. 2.4.

Contact analysis is applied to simulate the connection of components in the structures. No separation conditions are applied by using augmented Lagrange method. The contact types offered in ANSYS is shown in Table 2.1 [10].

2.4 Analysis Theories used in ANSYS Fluent

For the flow field, ANSYS Fluent solves conservation equations for both mass and momentum. In this thesis, the inviscid flow condition is assumed to derive the moment coefficient. Inviscid flow is the flow of an ideal fluid that is assumed to have no viscosity. In analysis, the effect of viscosity on the flow is neglected, so the inviscid flow analyses are appropriate for high-Reynolds-number applications where inertial forces tend to dominate viscous forces. [12]

In ANSYS Fluent, inviscid flow analyses solves the Euler equations. The equation for conservation of mass, or continuity equation can be expressed as follows:

$$\frac{\partial \rho}{\partial t} + \nabla \cdot (\rho \vec{v}) = S_m \tag{19}$$

Equation (19) is the general form of the mass conservation equation and is valid for incompressible as well as compressible flows. The source S_m is the mass added to the continuous phase from the dispersed second phase and any user-defined sources.

Conservation of momentum in an inertial reference frame is derived by Eq. (20).

$$\frac{\partial}{\partial t}(\rho\vec{v})+\nabla\cdot(\rho\vec{v}\,\vec{v})=-\nabla p+\nabla\cdot(\bar{\bar{\tau}})+\rho\vec{g}+\vec{F} \tag{20}$$

where p is the static pressure, $\bar{\bar{\tau}}$ is the stress tensor, and $\rho\vec{g}$ and $\vec{F}$ are the gravitational body force and external body forces, respectively. $\vec{F}$ also contains other model-dependent source terms such as porous-media and user-defined sources.

For two-dimensional axisymmetric geometries, the axial and radial momentum conservation equations are expressed as follows:

$$\frac{\partial}{\partial t}(\rho v_x)+\frac{1}{r}\frac{\partial}{\partial x}(r\rho v_x v_x)+\frac{1}{r}\frac{\partial}{\partial r}(r\rho v_r v_x)=-\frac{\partial p}{\partial x}$$
$$+\frac{1}{r}\frac{\partial}{\partial x}\left[r\mu\left(2\frac{\partial v_x}{\partial x}-\frac{2}{3}(\nabla\cdot\vec{v})\right)\right] \tag{21}$$
$$+\frac{1}{r}\frac{\partial}{\partial r}\left[r\mu\left(\frac{\partial v_x}{\partial r}+\frac{\partial v_r}{\partial x}\right)\right]+F_x$$

and

$$\frac{\partial}{\partial t}(\rho v_r)+\frac{1}{r}\frac{\partial}{\partial x}(r\rho v_x v_r)+\frac{1}{r}\frac{\partial}{\partial r}(r\rho v_r v_r)=-\frac{\partial p}{\partial r}$$
$$+\frac{1}{r}\frac{\partial}{\partial x}\left[r\mu\left(\frac{\partial v_r}{\partial x}+\frac{\partial v_x}{\partial r}\right)\right] \tag{22}$$
$$+\frac{1}{r}\frac{\partial}{\partial r}\left[r\mu\left(2\frac{\partial v_r}{\partial r}-\frac{2}{3}(\nabla\cdot\vec{v})\right)\right]$$
$$-2\mu\frac{v_r}{r^2}+\frac{2}{3}\frac{\mu}{r}(\nabla\cdot\vec{v})+\rho\frac{v_z^2}{r}+F_r$$

where $\nabla\cdot\vec{v}=\frac{\partial v_x}{\partial x}+\frac{\partial v_r}{\partial r}+\frac{v_r}{r}$ and v_z is the swirl velocity,.

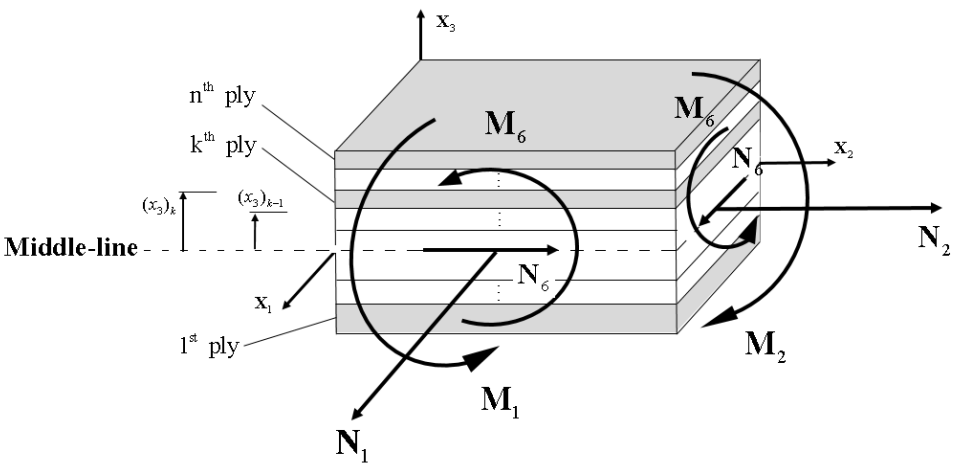

Figure 2.1. Classical Laminated Plate Theory[7]

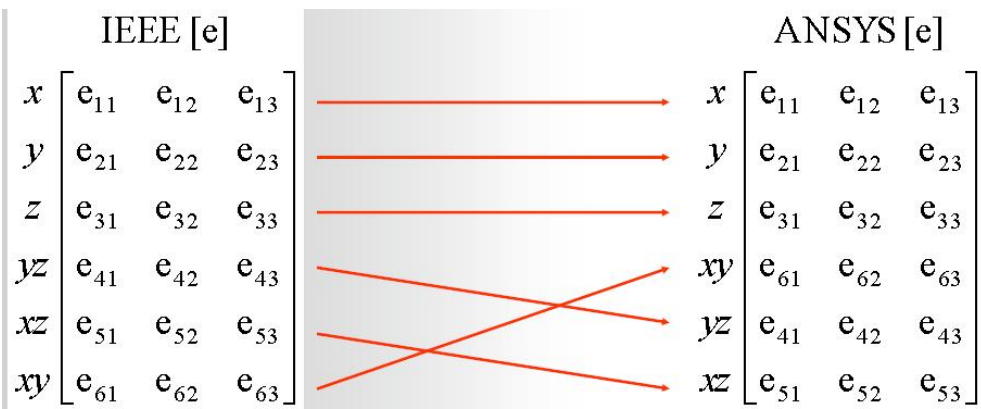

Figure 2.2. Piezoelectric Matrix in ANSYS[8]

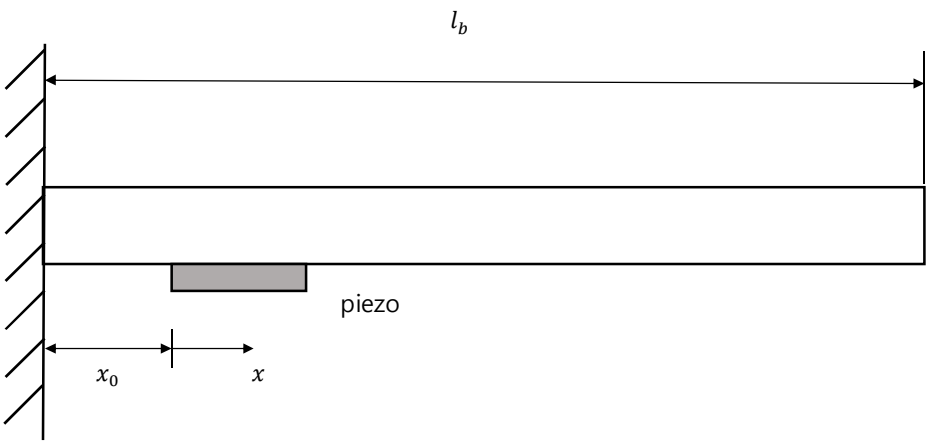

Figure 2.3. Single Surface-Mounted Piezo Actuator[9]

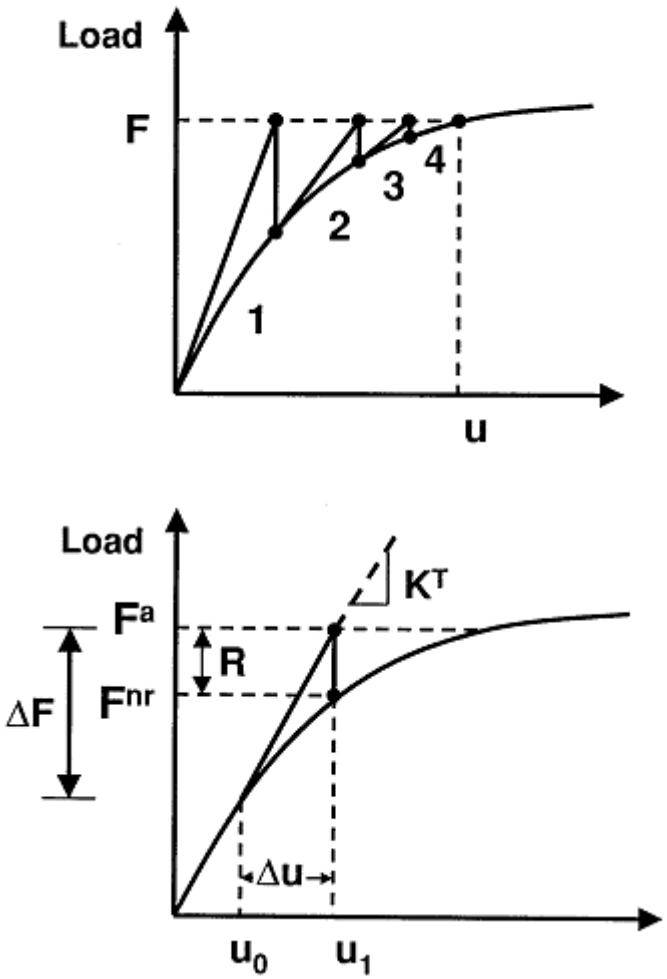

Figure 2.4. Newton Raphson Method [11]

Table 2.1. Summary of Contact Types and Options Available in ANSYS Simulation [10]

Contact Geometry	Solid Body Face (Scope = Contact)	Solid Body Edge (Scope = Contact)	Surface Body Face (Scope = Contact)	Surface Body Edge (Scope = Contact)
Solid Body Face	All types	Bonded, No Separation	Bonded, No Separation	Bonded only
	All formulations	All formulations	All formulations	MPC formulation
(Scope = Target)	Symmetry respected	Asymmetric only	Symmetry respected	Asymmetric only
Solid Body Edge	Not supported for solving[1]	Bonded, No Separation	Not supported for solving[1]	Bonded only
		All formulations		MPC formulation
(Scope = Target)		Asymmetric only		Asymmetric only
Surface Body Face	Bonded, No Separation	Bonded, No Separation	Bonded, No Separation	Bonded only
(Scope = Target)	All formulations	All formulations	All formulations	Augmented Lagrange, Pure Penalty, and MPC formulation
	Symmetry respected	Asymmetric only	Symmetry respected	Asymmetric only
Surface Body Edge	Not supported for solving[1]	Bonded only	Not supported for solving[1]	Bonded only
(Scope = Target)		MPC formulation		Augmented Lagrange, Pure Penalty, and MPC formulation
		Asymmetric only		Asymmetric only

1 – For Face/Edge contact, faces must always be designated as targets and edges must always be designated as contacts

III. Description of the Design Candidates for Smart Fin Structures

In this thesis, the smart fin structure is designed by referring Barret [4], and also further improved which is conducted and designed by previous researcher, Noh[13]. The smart fin structure is designed as a chord length 90mm and span length 60mm. The straight unimorph or bimorph actuator is embedded along the chordwise direction in the hollow inner space of airfoil. Piezoelectric material used in the smart fin structure is either 3203HD or PMN-29PT and is laminated to perform bending and extension actuation. The piezoelectric actuator is laminated asymmetrically with respect to mid-span regarding the unimorph actuator, which generates the bending moment. Bimorph actuator has symmetric composition of laminate, but bending is induced by applying an opposite voltage input on each piezoelectric actuator. Experiment is conducted regarding various laminated layers of actuators for performance comparison by Yoon[2].

3.1 Design Candidate 1

Instead of slanted actuator suggested by Barret[14], the straight unimorph and bimorph actuator were embedded along the chordwise direction in the hollow inner space of airfoil. It has a hinge at a 1/4 of chord which is constrained about its axial rotation. The actuator is separated from the smart fin in the initial state as shown in Fig. 3.2. When the voltage is applied on the actuator, the actuator will generate piezoelectric bending loads. Therefore the actuator will be in contact with projecting spot on the smart fin during actuation and the fin will be able to rotate along the pitch direction on a hinge. This design also adopts bearing to rotate smoothly. The material used in this design is shown in Table 3.1

The actuator used in this concept is designed as unimorph and bimorph type.

Unimorph actuator has five laminated layers, and the piezoelectric material is layered asymmetrically with respect to mid-span. Then, if the voltage is generated in the piezoelectric material, it will induce the extension along the longitudinal direction, and its extension will generate the bending moment at the piezoelectric actuator. Bimorph actuator has three laminated layers, and the piezoelectric material is layered symmetrically on both sides with respect to mid-span. The bending moment of bimorph actuator is induced by applying opposite voltage input at each piezoelectric material. The piezoelectric material used this design concept is PMN-29PT. Figure 3.5 shows the laminated layers of both unimorph and bimorph actuator.

3.2 Design Candidate 2

Similar to Design Candidate 2, the straight unimorph actuator is embedded along the chordwise direction in the hollow inner space of the airfoil. However, the additional geometric component called the support component is added between the actuator tip and airfoil to reduce the loss of bending moment of the actuator caused by the geometry of Design Candidate 1. Because the actuator is not bonded at the airfoil, it does not incur torsional effect so the bending moment of the actuator can completely transfer the rotation effect of the airfoil. It also adopts bearing to rotate smoothly. The actuator used in Design Candidate 2 is similar to the unimorph actuator used in Design Candidate 1. However, piezoelectric material called 3203HD was used in Design Candidate 2 instead of PMN-29PT.

3.3 Design Candidate 3

Design Candidate 3 is suggested to enable symmetrically performance of the smart fin. It is similar to the original design, but two actuators are placed symmetrically along the spanwise direction in the hollow airfoil fin. If the pitch

rotation angle of the smart fin increases, contact occurs between the actuator and smart fin during actuation [15]. Therefore, the airfoil is re-designed as a taper shape to solve its geometry limit by applying NACA0015 at the root airfoil and NACA0012 at the tip airfoil.

Piezoelectric material used in the actuator is PMN-29PT. PMN-29PT is also used in the actuator in Design Candidate 1, however, the actuating direction is differ. In Design Candidate 1, the dielectric direction is set in 1-direction, in contrast, 2-direction actuation is applied in Design Candidate 3. Because the dielectric constant and elastic modulus in 2-direction (d_{32}) is larger than those in 1-direction (d_{31}), the tip deflection of the actuator used in Design Candidate 3 is almost 4 times larger than that in Design Candidate 1 [16].

In Design Candidate 3, the only one actuator is in operation. The remaining one is not in operation and acts as a dummy actuator. To reduce the dummy effect during actuation, the additional structural component is applied at root of the actuator. To simulate such situation, the material properties of the dummy actuator was reduced to be 1/100 of its original values in order to artificially avoid a possible resistance by the dummy actuator by comparing the experiment result [17].

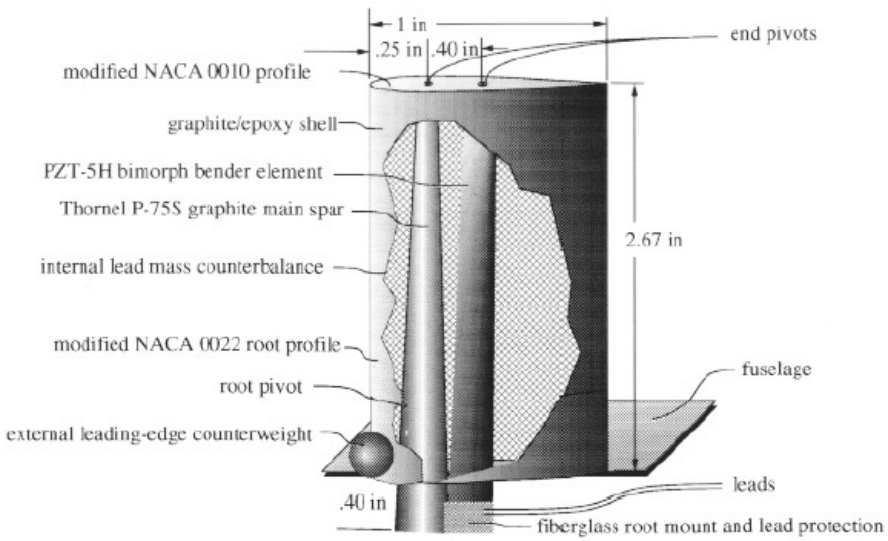

Figure 3.1 Design of the Flexspar Missile Wing [14]

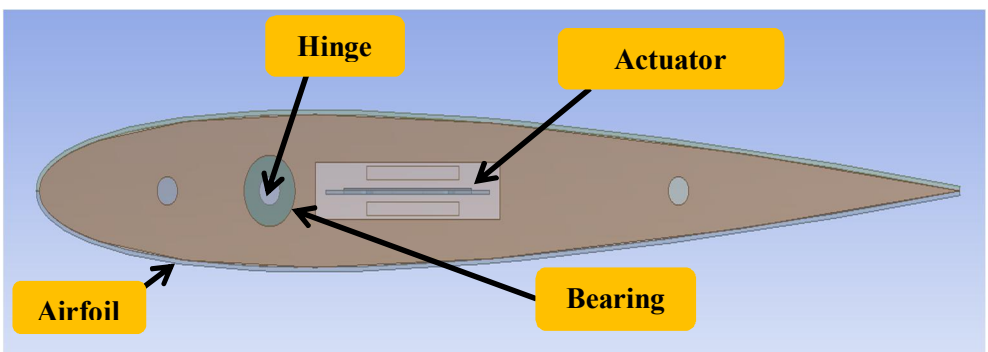

Figure 3.2 Cross-sectional View of Design Candidate 1

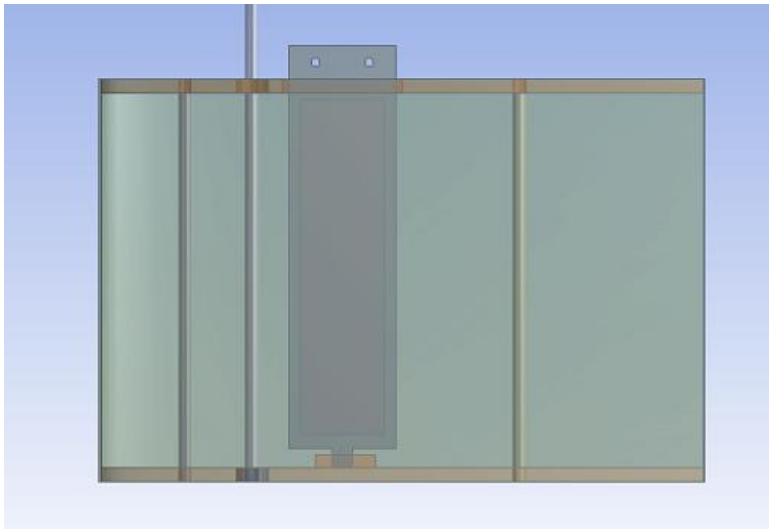

(a) Upper View

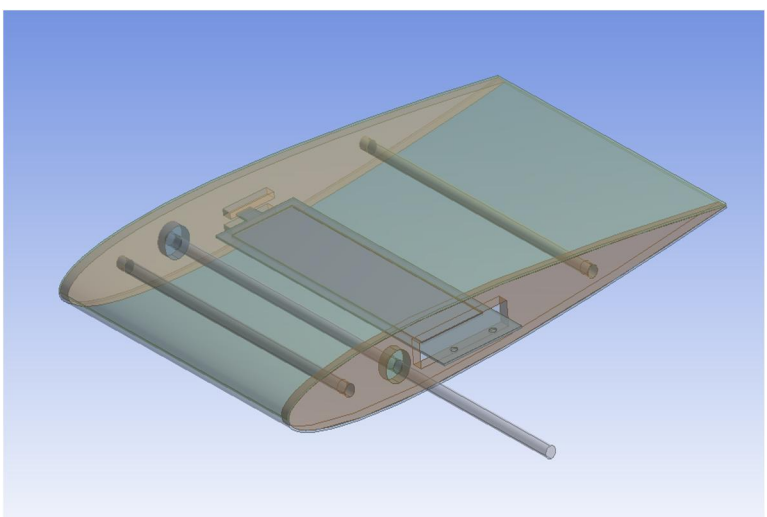

(b) Isometric View

Figure 3.3 Upper and Isometric View of Design Candidate 1

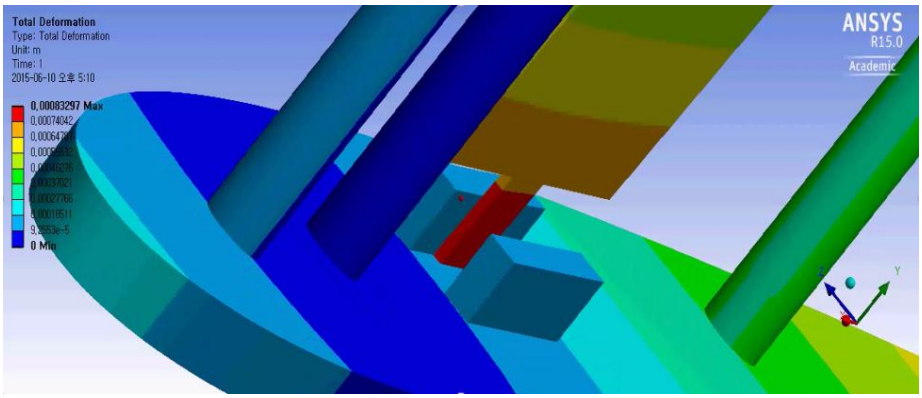

Figure 3.4 Projecting Spot on the Smart Fin during Actuation

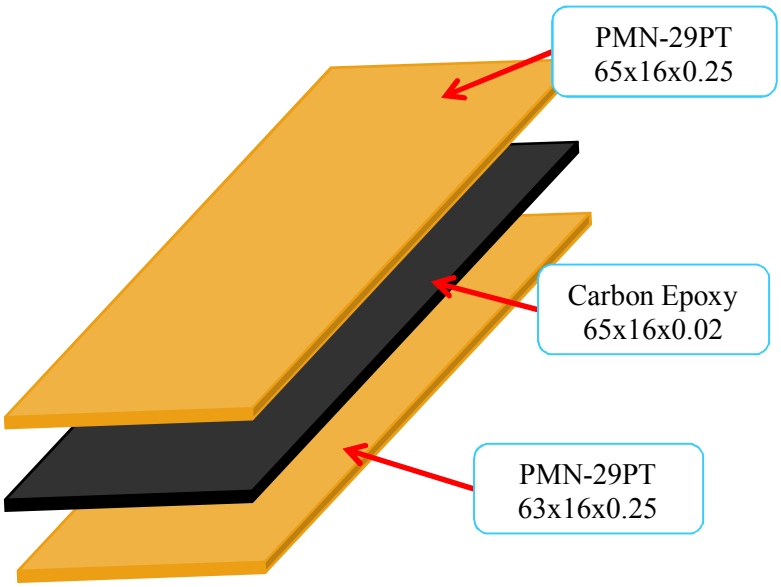

(a) Bimorph Actuator

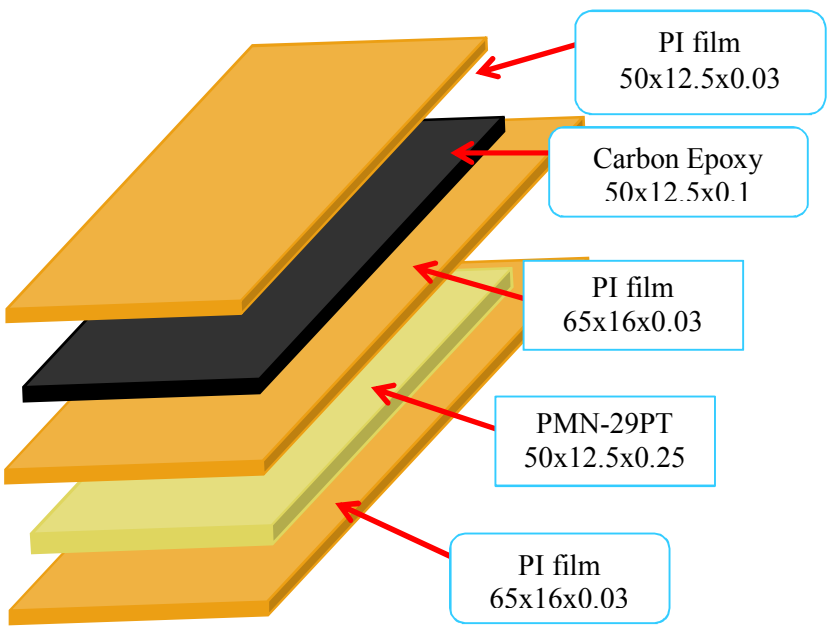

(b) Unimorph Actuator

Figure 3.5 Lay-up and Dimension of the Bimorph and Unimorph Actuators in Design Candidate 1

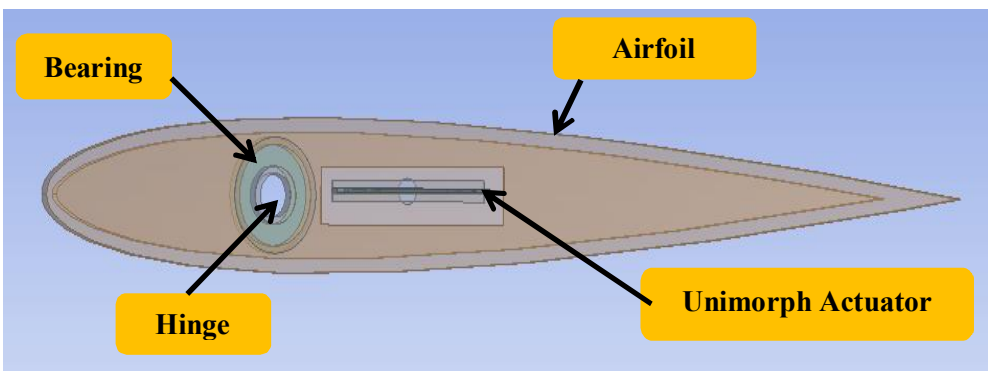

Figure 3.6 Cross-sectional View of Design Candidate 2

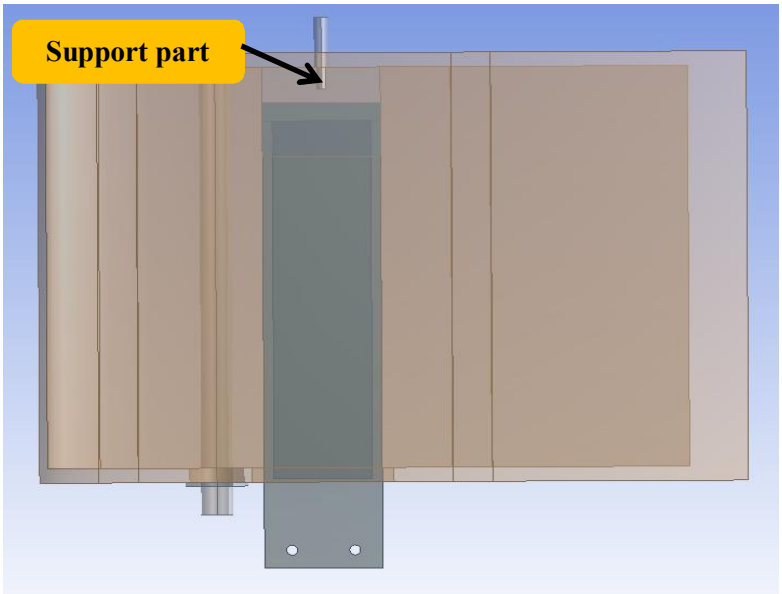

(a) Upper View

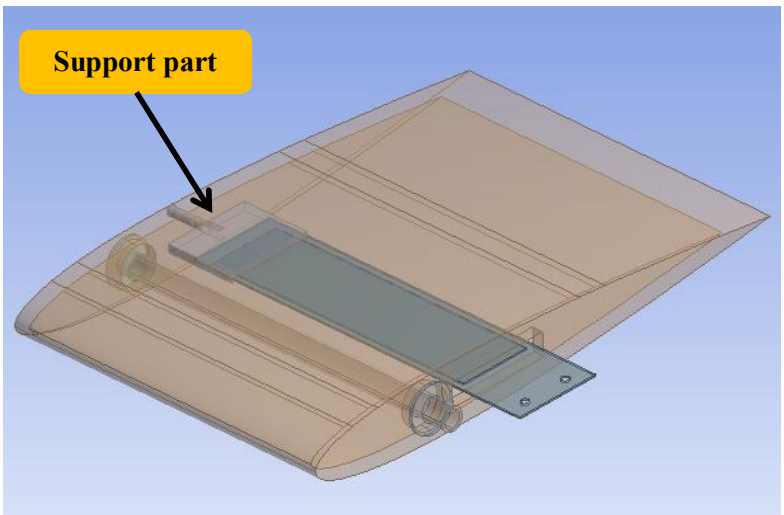

(b) Isometric View

Figure 3.7 Upper and Isometric View of Design Candidate 2

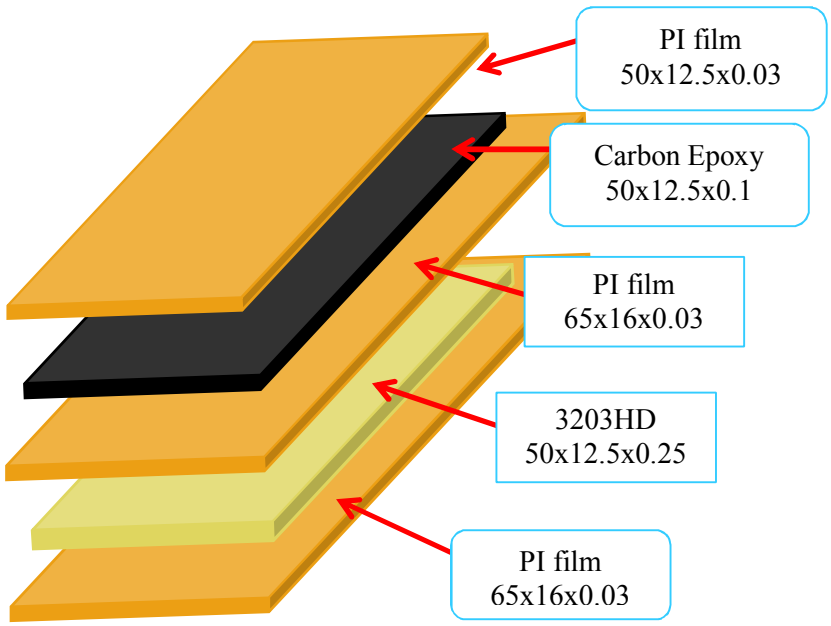

Figure 3.8 Lay-up and Dimension of the Unimorph Actuator in Design Candidate 2

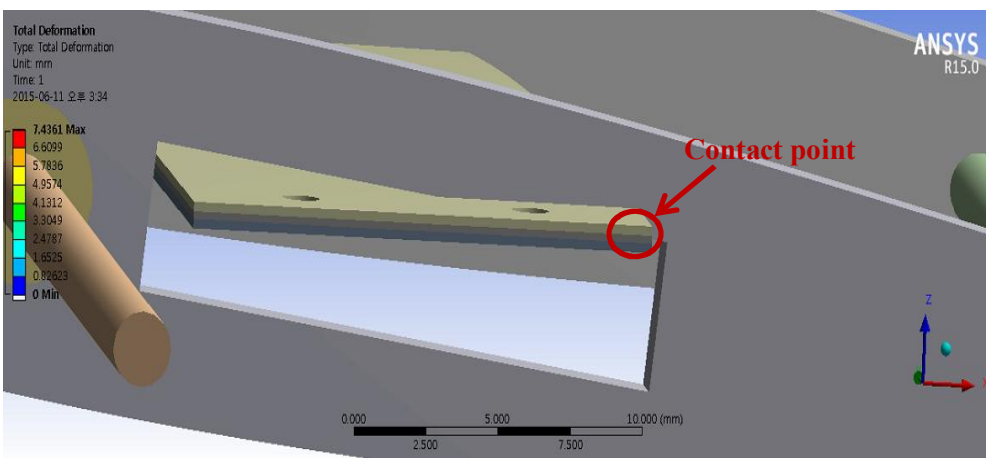

Figure 3.9 Geometry Limit of Design Candidate 2

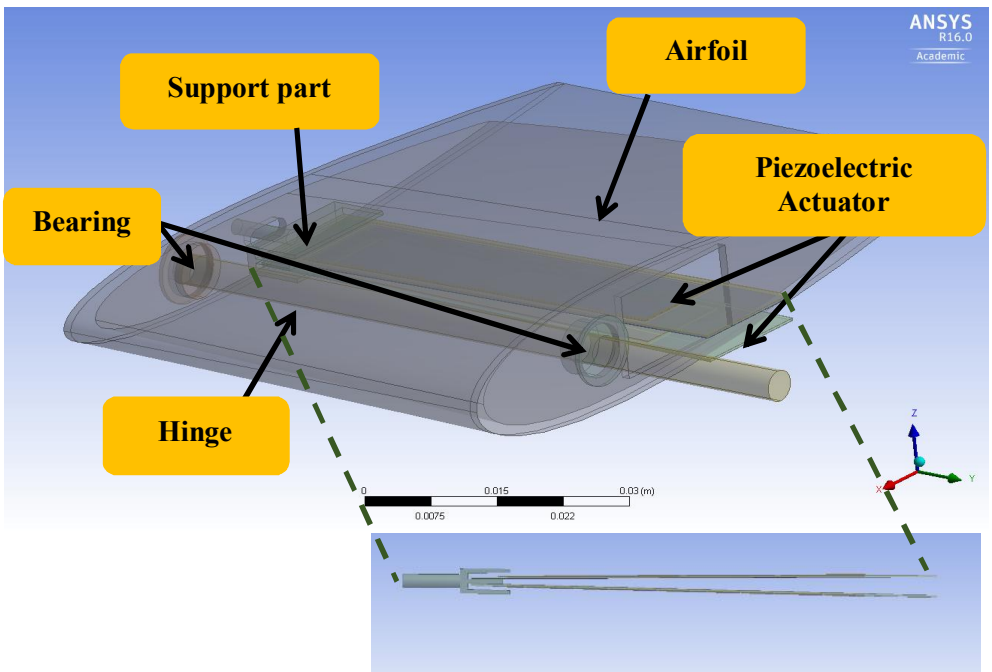

Figure 3.10 Isometric view of Design Candidate 3

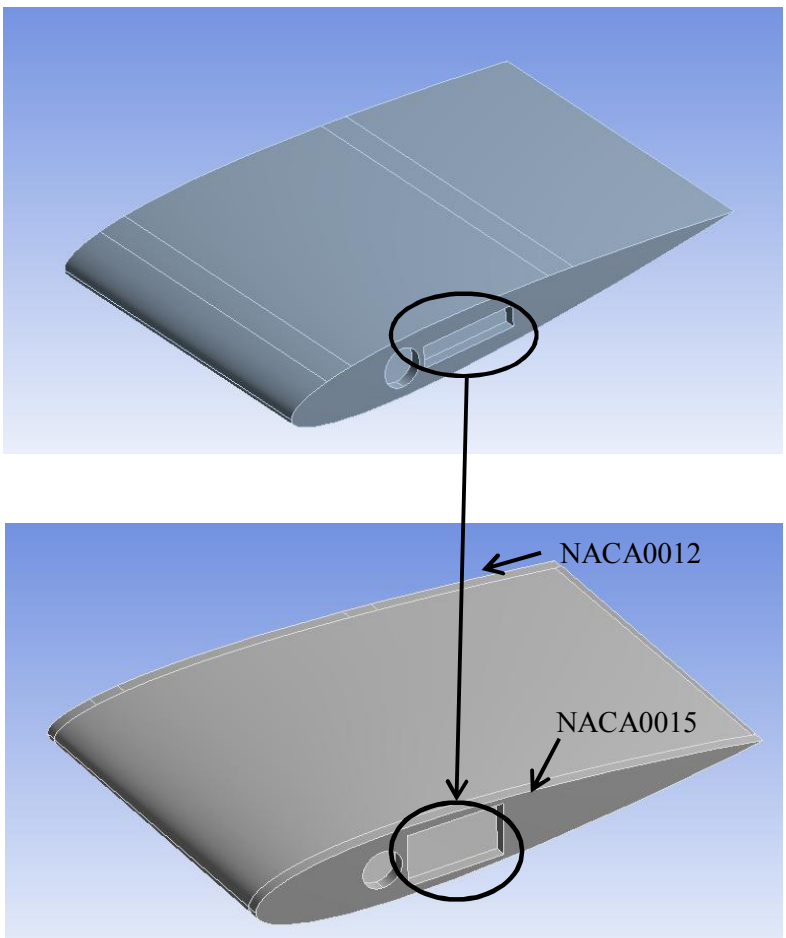

Figure 3.11 Geometry Improvement of the Hollow Airfoil Fin

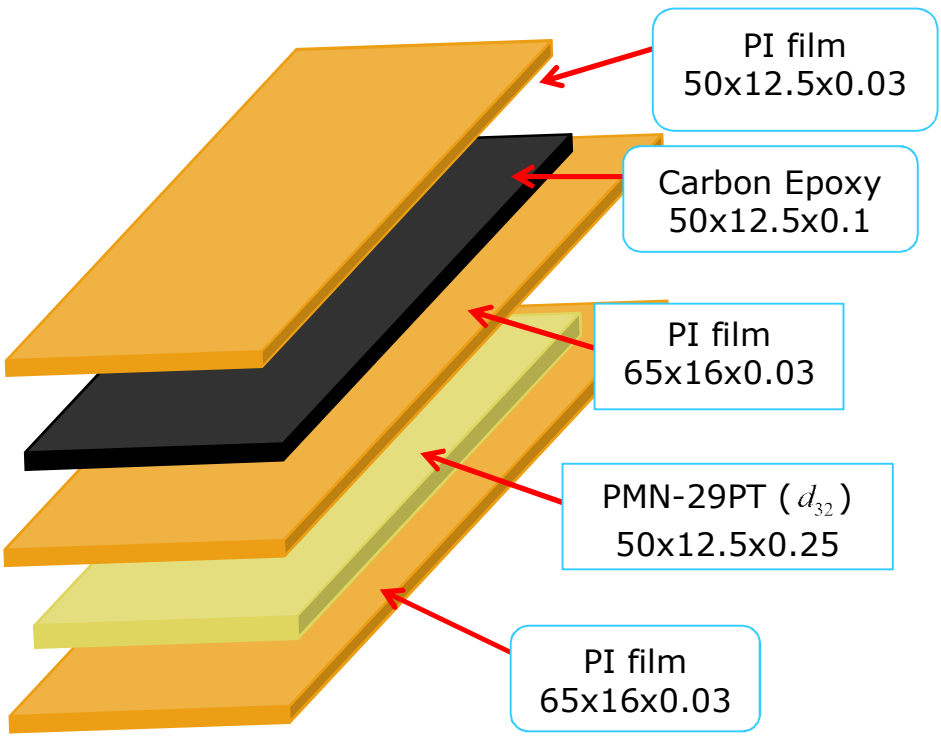

Figure 3.12 Lay-up and Dimension of the Unimorph Actuator in Design Candidate 3

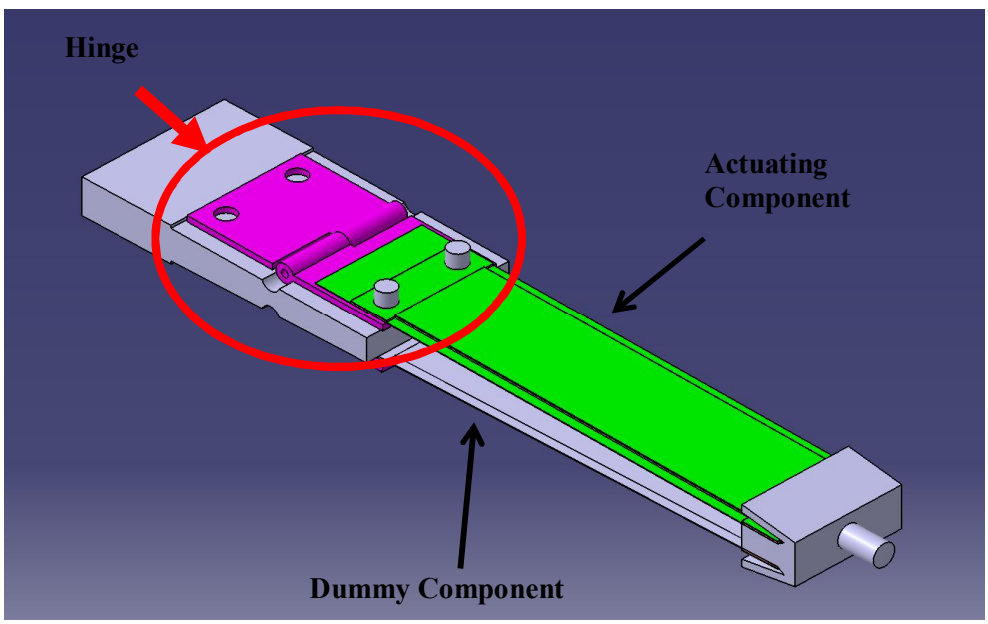

Figure 3.13 Additional Structural Component applied at the Root of the Actuators

Table 3.1 Material Properties used in the Design Candidate 1 [18]

	Parts	Material/ Lay-up	Material Property
1	Airfoil	Aluminum-alloy	$E = 71GPa, v = 0.33$
2	Skin	Glass/Epoxy	$E_1 = 21.7GPa, v = 0.3$
3	Hinge	Carbon/Epoxy	$E_1 = 217.2GPa, v = 0.29$
4	Front/Back spar	Carbon/Epoxy	$E_1 = 217.2GPa, v = 0.29$
5	Bearing	Aluminum-alloy	$E = 71GPa, v = 0.33$
6	Unimorph Actuator	PI film	$E_1 = 3GPa, v = 0.3$
		Carbon/Epoxy	$E_1 = 217.2GPa, v = 0.29$
		PI film	$E_1 = 3GPa, v = 0.3$
		PMN-29PT	$E_1 = 44GPa, v = 0.3$
		PI film	$E_1 = 3GPa, v = 0.3$
7	Bimorph Actuator	PMN-29PT	$E_1 = 44GPa, v = 0.3$
		Carbon/Epoxy	$E_1 = 217.2GPa, v = 0.29$
		PMN-29PT	$E_1 = 44GPa, v = 0.3$

Table 3.2 Material Properties used in the Design Candidate 2

	Parts	Material/ Lay-up	Material Property
1	Airfoil/Skin	ULTEM	$E = 3.6GPa, v = 0.36$
2	Hinge	Carbon/Epoxy	$E_1 = 217.2GPa, v = 0.29$
3	Support part	Carbon/Epoxy	$E_1 = 217.2GPa, v = 0.29$
4	Bearing	Aluminum-alloy	$E = 71GPa, v = 0.33$
5	Unimorph Actuator	PI film	$E_1 = 3GPa, v = 0.3$
		Carbon/Epoxy	$E_1 = 217.2GPa, v = 0.29$
		PI film	$E_1 = 3GPa, v = 0.3$
		3203HD	$E_1 = 60.2GPa, v = 0.25$
		PI film	$E_1 = 3GPa, v = 0.3$

Table 3.3 Material Properties used in the Design Candidate 3

	Parts	Material/ Lay-up	Material Property
1	Airfoil/Skin	Polycarbonate	$E = 2.2Gpa, v = 0.37$
2	Hinge	Carbon/Epoxy	$E_1 = 217.2Gpa, v = 0.29$
3	Support part	Carbon/Epoxy	$E_1 = 217.2Gpa, v = 0.29$
4	Bearing	Aluminum-alloy	$E = 71Gpa, v = 0.33$
5	Unimorph Actuator	PI film	$E_1 = 3GPa, v = 0.3$
		Carbon/Epoxy	$E_1 = 217.2GPa, v = 0.29$
		PI film	$E_1 = 3GPa, v = 0.3$
		PMN-29PT	$E_1 = 44GPa, v = 0.3$
		PI film	$E_1 = 3GPa, v = 0.3$

Table 3.4 Comparison of Elastic Constants and Dielectric Constants between PMN-29PT and 3203HD [16, 19]

Material	Elastic Constant	Dielectric constant
3203HD	$\mathrm{E}_1 = 60.2GPa$	$\mathrm{d}_{31} = -320\mathrm{m/V} \times 10^{-12}$
PMN-29PT	$\mathrm{E}_1 = 44GPa$	$\mathrm{d}_{31} = 437.3\mathrm{m/V} \times 10^{-12}$
	$\mathrm{E}_2 = 8.9GPa$	$\mathrm{d}_{32} = -1350\mathrm{m/V} \times 10^{-12}$

IV. Numerical and Experimental Results

Structural analysis for the smart fin embedded with piezoelectric material is conducted using commercial finite element method analysis software, ANSYS. Solutions from ANSYS provide the simulation about every structural aspect of a product, including linear static analyses that simply provide stresses and deformations, modal analysis that determines vibration characteristics, to advanced transient nonlinear phenomena involving effects and complex behaviors. Analysis of the design candidate was conducted two aspects. One is applying voltage at the actuator by using Piezo and MEMS module provided in ANSYS [8]. The other is applying the equivalent bending moment at the actuator by using the smart structure theory [9].

To predict the resulting rotation of pitch angle of the smart fin, the aerodynamic hinge moment and actuator torque is predicted by using ANSYS Fluent and Structural analysis. To estimate the actuator torque, fixed support prescribes at the trailing edge of the smart fin and the reaction force is evaluated. In that process, the aerodynamic hinge moment and actuator torque is assumed that both are linearly related to the rotating angle. By plotting a graph regarding the moment and rotation angle, the final resulting rotation of pitch angle is obtained.

4.1 Piezoelectric Actuator

In order to verify the performance of the present piezoelectric actuator, experimental result of actuator actuation is compared with analytical result when voltage is applied and equivalent bending moment is applied by using ANSYS.

The target actuator for deriving those three results is unimorph actuator using PMN-29PT actuating in 1-direction when 400 volt is applied. Comparison of those three results shows in Table 4.1 and experimental result shows good correlation with analysis result when voltage and equivalent bending moment is applied. The performance angle of piezoelectric actuator is calculated by using inverse tangent. Because both unimorph and bimorph actuator generate the bending moment, the actuators moves along z-direction. So through its length and deformation along z-direction, the performance angle can be calculated as shown in Fig. 4.1.

To improve the performance of smart fin, three lay-up types of piezoelectric actuator is designed as shown in Fig. 4.4. Although the performance angle of bimorph actuator is better than that of unimorph actuator, those three actuators are designed as unimorph type because voltage coupling problem occur when bimorph actuator uses in experiment. All the piezoelectric actuators is designed as five layers, however, the piezoelectric material and actuating direction is differ. Piezoelectric material 3203HD actuates in 1-direction, in contrast, PMN-29PT actuates in 2-direction. In Table 4.2, the actuator using PI film and PMN-29PT has performance angle of 6.2° and it shows three times larger performance angle value than other actuators. Thus, in Design Candidate 3, its actuator is used to analyze and experiment the resulting pitch rotation angle of smart fin.

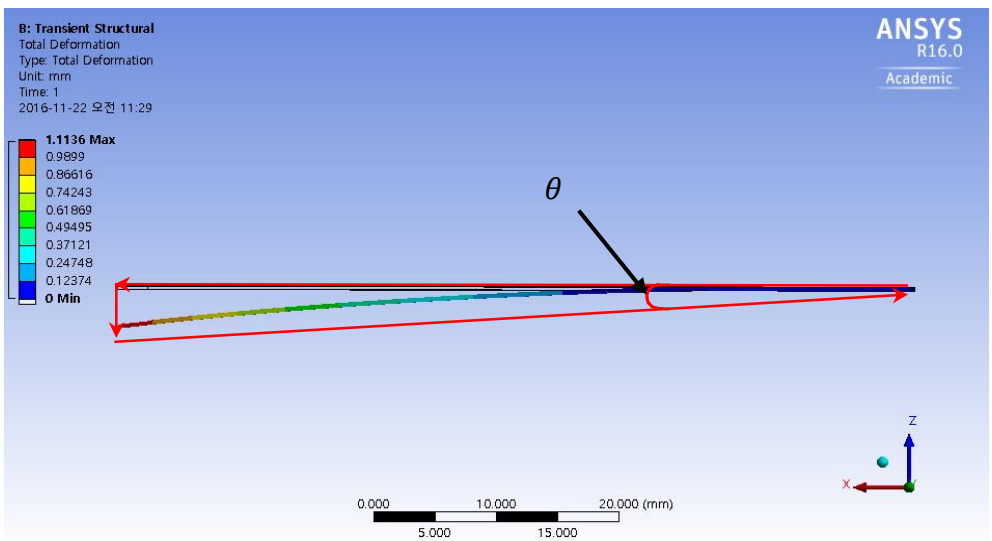

Figure 4.1 Estimation on Rotation Angle of Actuator using Inverse Tangent

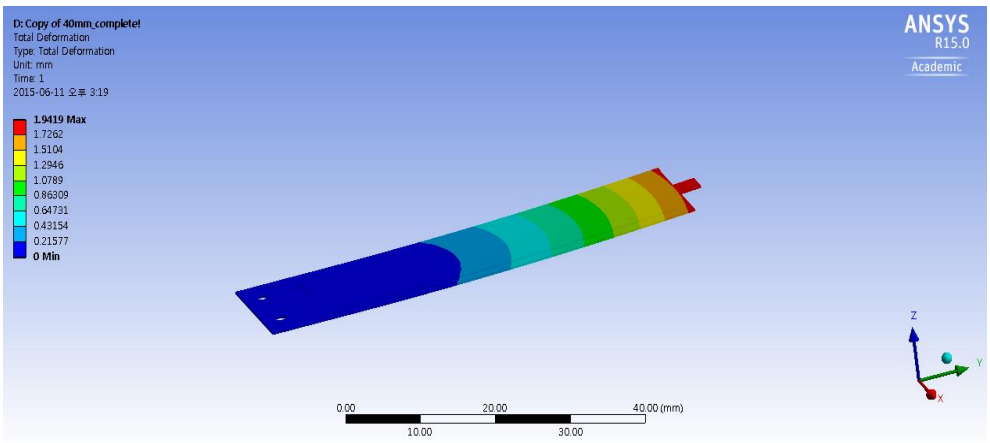

(a) Result of Unimorph Actuator in Design Candidate 1

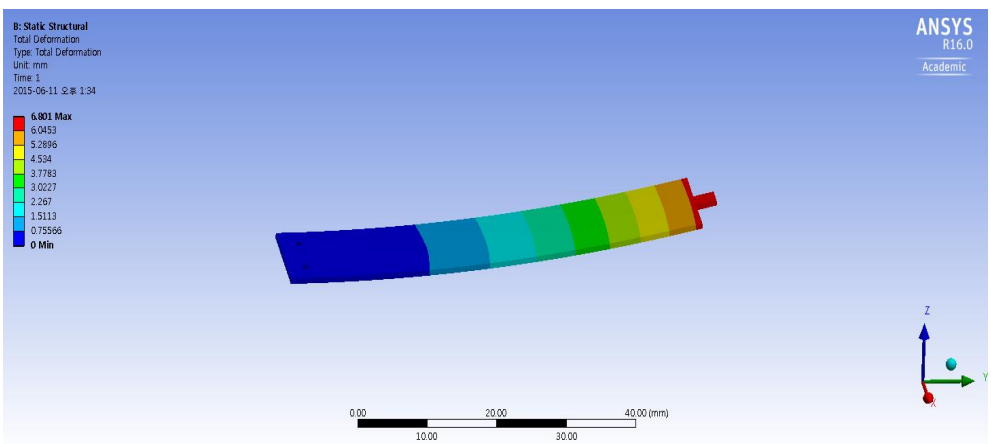

(b) Result of Bimorph Actuator in Design Candidate 1

Figure 4.2 Result of Rotation Angle of Actuators used in Design Candidate 1

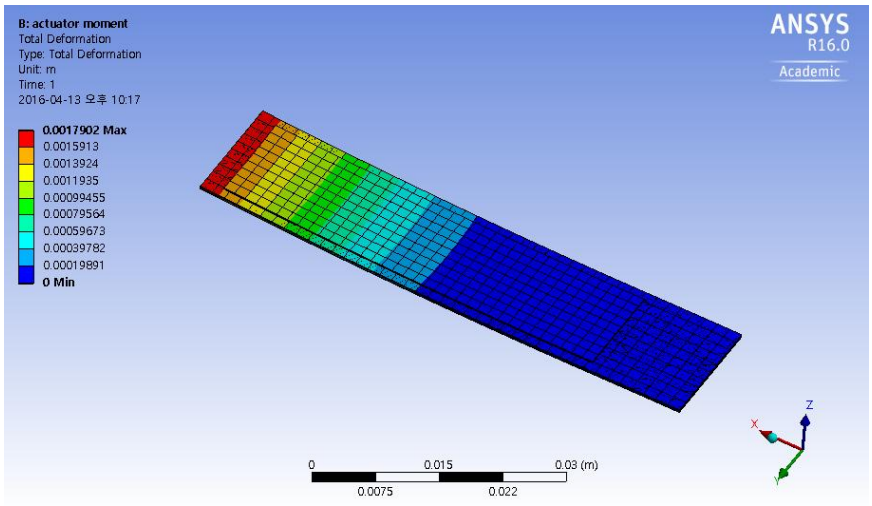

(a) Result of Unimorph Actuator using 3203HD

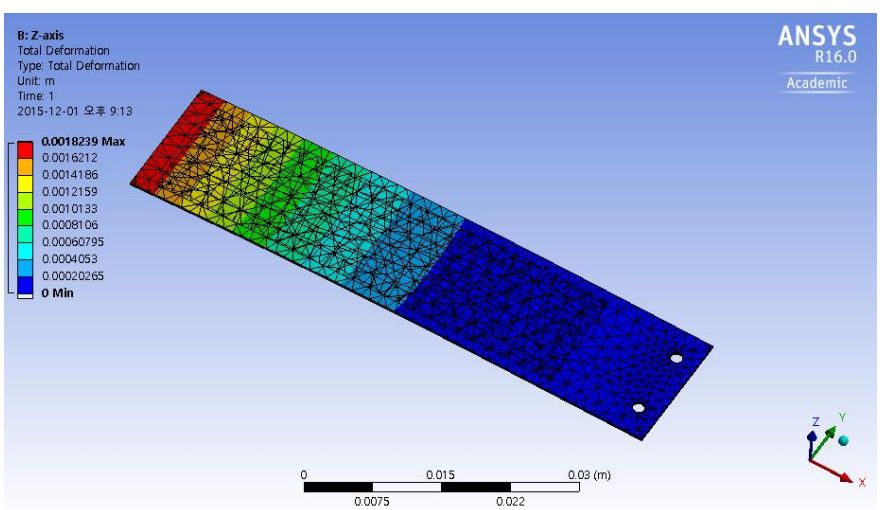

(Equivalent bending moment)

(b) Result of Unimorph Actuator using 3203HD

(Voltage input)

Figure 4.3 Comparison Rotation Angle of Unimorph Actuator when using Equivalent Bending Moment and Voltage Input

Polyimide film	Polyimide film	Glass/Epoxy
Carbon/Epoxy	Carbon/Epoxy	Carbon/Epoxy
Polyimide film	Polyimide film	Glass/Epoxy
3203HD(d_{31})	PMN-29PT(d_{32})	PMN-29PT(d_{32})
Polyimide film	Polyimide film	Glass/Epoxy

Figure 4.4 Design of Three Lay-up Types of Unimorph Actuators for Performance Improvement

Table 4.1 Comparison of Rotation Angle of Unimorph Actuators Using 3203HD among Experiment and Analysis

	Rotation Angle
Analysis result (Voltage Input)	1.63°
Analysis Result (Equivalent Bending Moment)	1.58°
Experiment Result	1.6°

Table 4.2 Comparison of Rotation Angle of Unimorph Actuators for Performance Improvement

	Experiment	**ANSYS**
PMN-29PT/Glass Epoxy (d_{32})	1.72°	1.15°
PMN-29PT/PI film (d_{32})	5°	6.19°
3203HD/PI film	1.6°	1.78°

4.2 Structural Analysis of the Present Smart Fin

In structural analysis, rotation of pitch angle of the smart fin is predicted when aerodynamic load is not applied by using ANSYS Structural. In Design Candidate 1 and 2, 400 volt is applied on the actuator and rotation of pitch angle of the smart fin is measured by using PIEZO and MEMS module. In Design Candidate 3, the equivalent bending moment is calculated and applied at piezoelectric actuator to measure rotation of pitch angle. Both voltage input and equivalent bending moment is given linearly from time 0 to 1 sec. The rotation of pitch angle is calculated by using inverse tangent, considering the deflection of trailing edge and length between trailing edge and hinge.

4.2.1 Design Candidate 1

The actuator is located at 0.4 of chord line and 400 volt is applied on piezoelectric material. Actuator is separated from the smart fin in the initial configuration. Then it will be in contact with projecting spot on the smart fin during actuation and pin will rotate on a hinge. To realize the frictional contact on that spot and rotation hinge, the structural behavior is analyzed using the relevant nonlinear formulation provided in ANSYS. Augmented Lagrange formulation and pinball condition is used to prevent the penetration in the contact region and solve several iterations at each time step until penetration do not occur [11].

The rotation of pitch angle of Design Candidate 1 is found to be 0.55° when using unimorph actuator. When using the bimorph actuator, the rotation of pitch

angle is increased as 6.31°. 400 volt is applied on the upper component of piezoelectric actuator and 0 volt on the lower component. Because rotation of pitch angle of the smart fin has large value, contact problem occurs between the actuator and smart fin during actuation as shown in Fig. 4.6. Also, the bimorph actuator has problems during actuation in experiment because of voltage coupling. Also actuating mechanism of Design Candidate 1 has loss of actuating force because the actuator and smart fin is separated at the initial state. Therefore, modified design concepts such as Design Candidate 2 and 3 are suggested to supplement those problems like the geometry limit and loss of the actuator bending force during actuation.

4.2.2 Design Candidate 2

To solve loss of the actuator bending force during actuation, the additional component called the support component is now added between the airfoil and actuator. Small hole makes to insert the support part at the tip airfoil. Because connection between the support component and airfoil has no gap and is not bonded, bending moment generated at the unimorph actuator can transfer torque of the airfoil. Therefore, the loss of actuator bending force can decrease compared with Design Candidate 1. Piezoelectric material used in Design Candidate 2 is 3203HD which has larger elastic constant than PMN-29PT. The unimorph actuator is located at 0.4 of chord line and 400 volt is applied on the piezoelectric material. With the linear increase of voltage input of 400 volt over 1 sec without external load, the rotation of pitch angle is 3.71° at the trailing edge.

In Design Candidate 2, stability analysis and structural response simulations of the smart fin control system is performed in Kang [20]. Stability analysis such as flutter analysis is conducted by integrating MSC.NASTRAN and ZAERO, and structural response simulations is performed by using result of stability analysis

and MATLAB/Simulink. In the process, modal analysis of the present smart fin design is first conducted and flutter speed is predicted by plotting *V-g* and *V-f* plot. In structural response simulations, PI controller is designed to increase the flight stability speed and to maintain the rotation of pitch angle of the smart fin under a specific flight speed condition. PI controller is designed by using PID Tuner supported to MATLAB/Simulink. And then, the complete closed-loop system for structural response simulation is constructed and analyzed by using both ZAERO and MATLAB/Simulink. The flutter speed is predicted as 282m/s in open-loop system, and the flutter mode is the first natural mode. In closed-loop system, flutter speed is found to be 350m/s, increased by about 24% than that from open-loop system. Also, the settling time of the step responses of the smart fin is decreased as 0.1 seconds.

In fact, the unimorph actuator is designed unsymmetrically, its actuation along z-direction is also unsymmetrical. Therefore, Design Candidate 3 is suggested for symmetrical actuation and to solve geometric limit of the smart fin referred to Design Candidate 1.

4.2.3 Design Candidate 3

In Design Candidate 3, the support component is also added to prevent loss of the actuator bending force during actuation. The hollow airfoil fin is designed as a taper shape by applying NACA0015 at the root airfoil and NACA0012 at the tip airfoil which is explained in Section 3. Also, two actuator is applied symmetrically along the chord of airfoil for symmetric actuation on both upper and bottom direction. In this evaluation, it is assumed that only one actuator is in operation. Single-crystal piezoelectric material called PMN-29PT is used instead of 3203HD for increasing the performance of the smart fin as shown in Table 4.2. The equivalent bending moment is applied on the piezoelectric material. With linear

increase of bending moment over 1 sec without external load, the rotation of pitch angle is 4.1° at the trailing edge.

To improve the performance of the smart fin and decrease the effect of resistance caused by dummy actuator, the modified structure design is introduced which is explained in Section 3. To simulate such situation in ANSYS, the material properties of the dummy actuator was reduced to be 1/100 of its original values in order to artificially avoid a possible resistance by the dummy actuator. In this case, bending moment is also increased linearly over 1 sec without external load, then the rotation of pitch angle is 10.6° at the trailing edge. Compared with previous result, the rotation performance is increased more than two times.

In this section, all analysis regarding rotation performance of the smart fin is conducted when aerodynamic load is not applied. In real system, the aerodynamic effect during flight condition is important and it affects the rotation performance of the smart fin during actuation. Therefore, in next section, performance rotation analysis of the smart fin is conducted when the aerodynamic effect is considered in the case of Design Candidate 3.

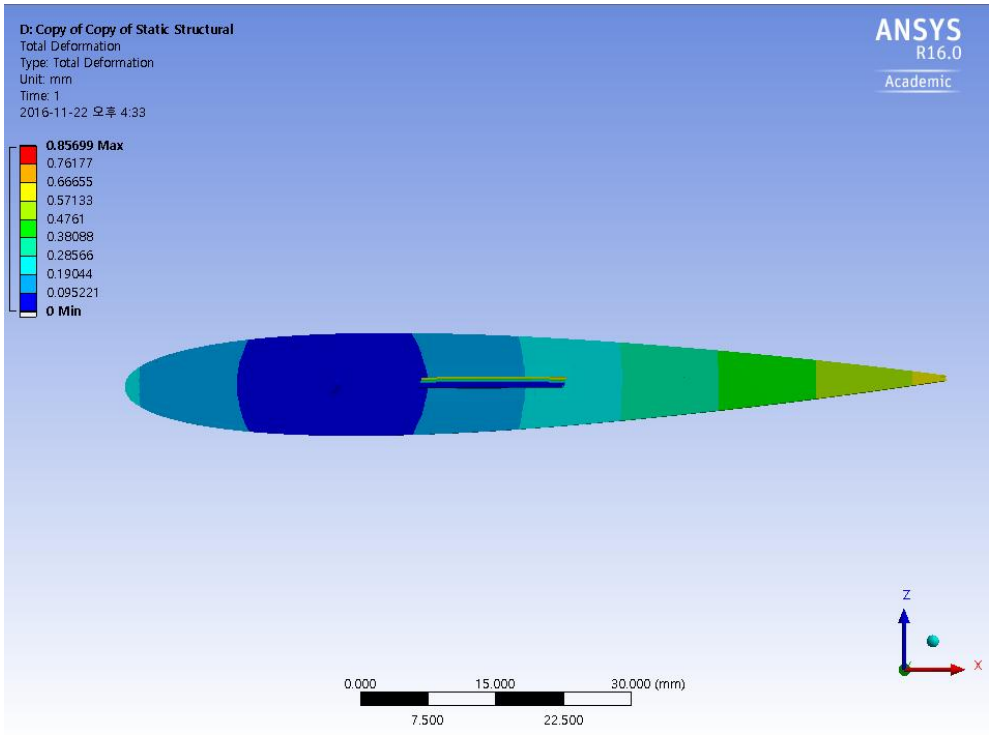

Figure 4.5 Rotation Result of Design Candidate 1 using Unimorph

Actuator

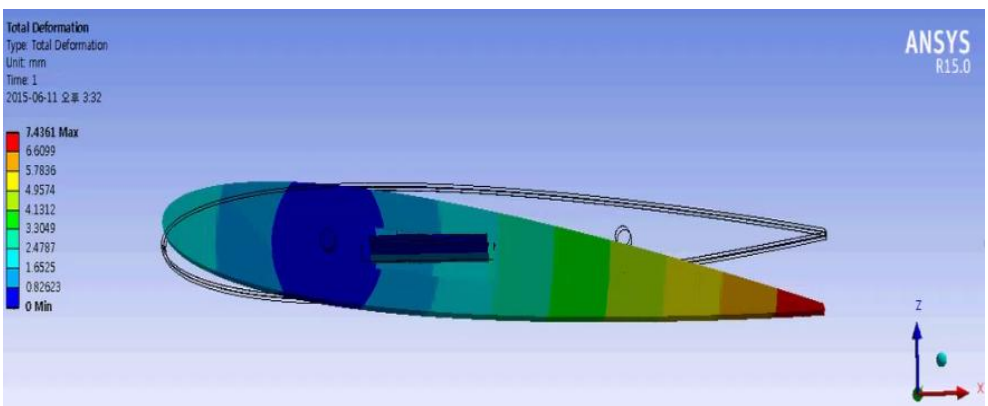

(a) Rotation Result of Smart Fin

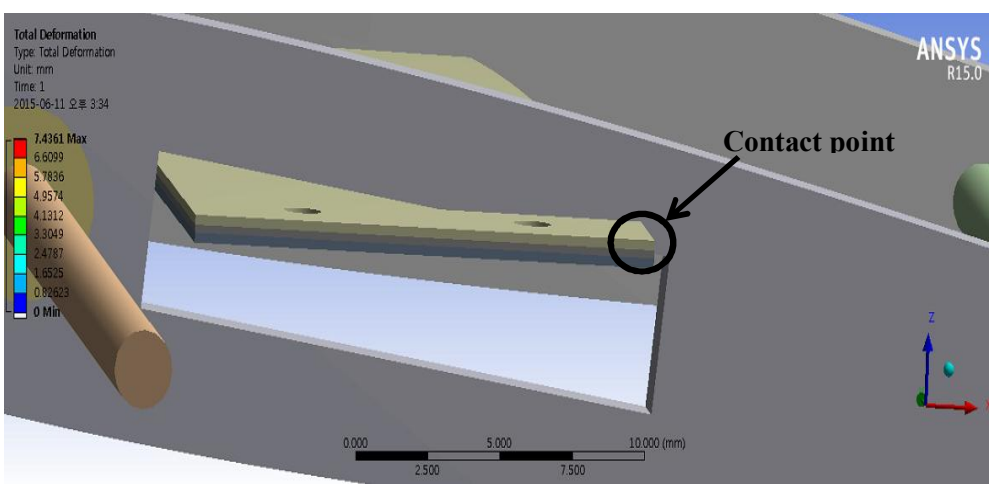

(b) Geometry Limit of Smart Fin

Figure 4.6 Rotation Result of Design Candidate 1 using Bimorph Actuator and Geometry Limit of Design Candidate 1

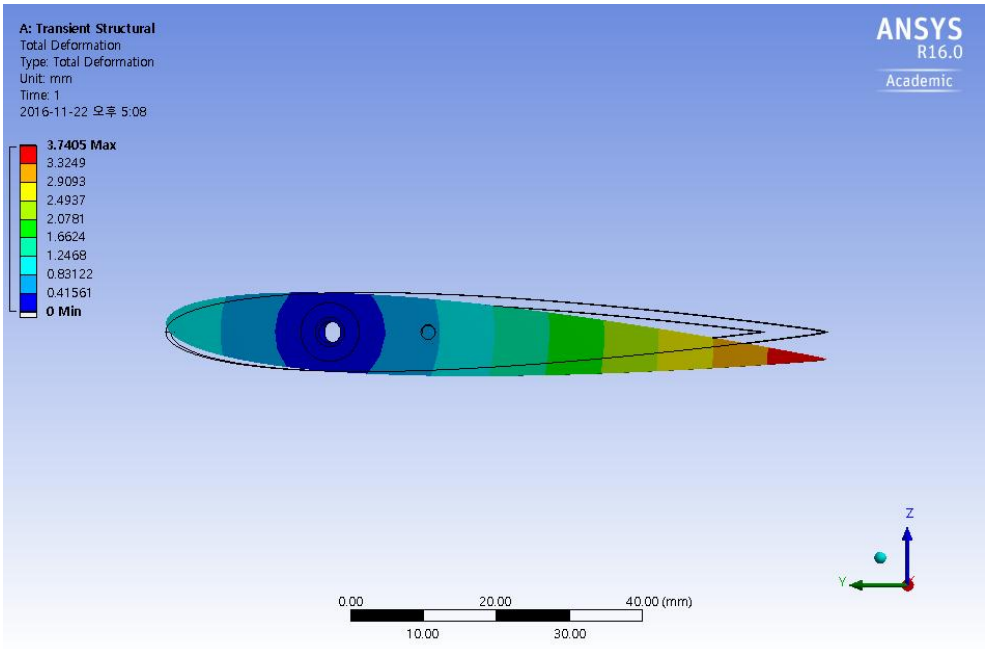

Figure 4.7 Rotation Result of Design Candidate 2

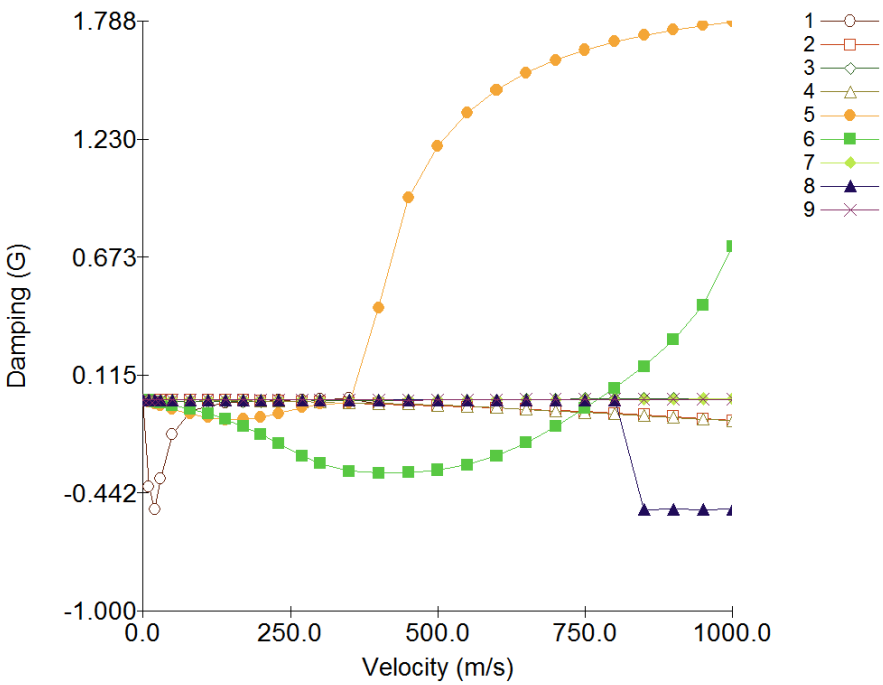

(a) V-g plot for Flutter Stability

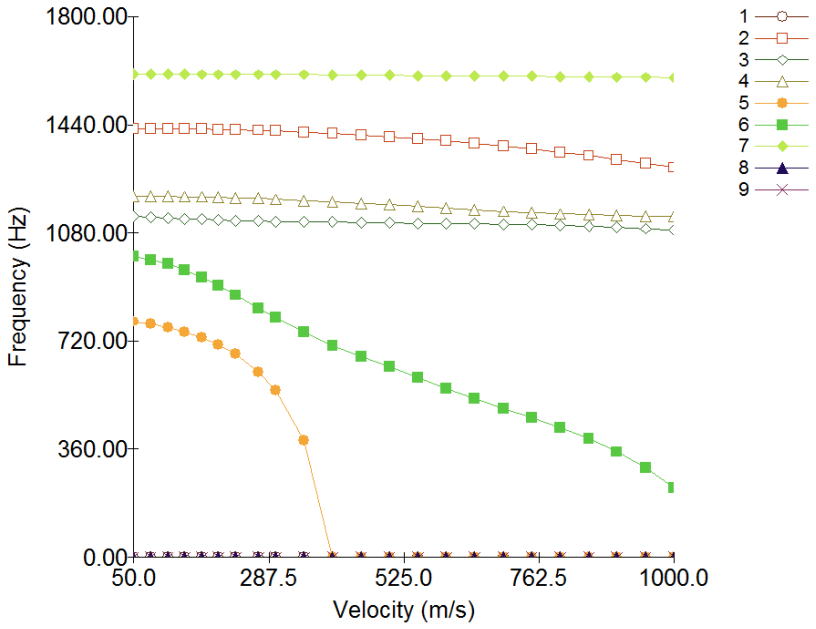

(b) V-f plot for Flutter Stability

Figure 4.8 V-g and V-f plot for Flutter Stability using *g*-method [20]

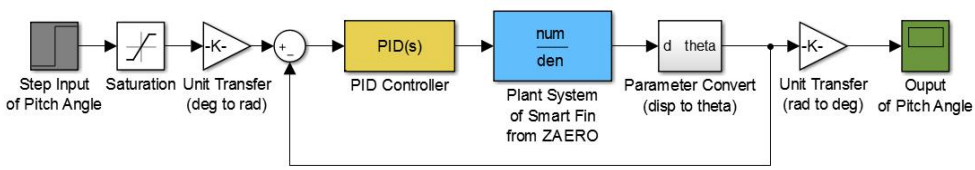

Figure 4.9 Closed-loop System for Aeroservoelastic Smart Fin Control Constituted in MATLAB/Simulink [20]

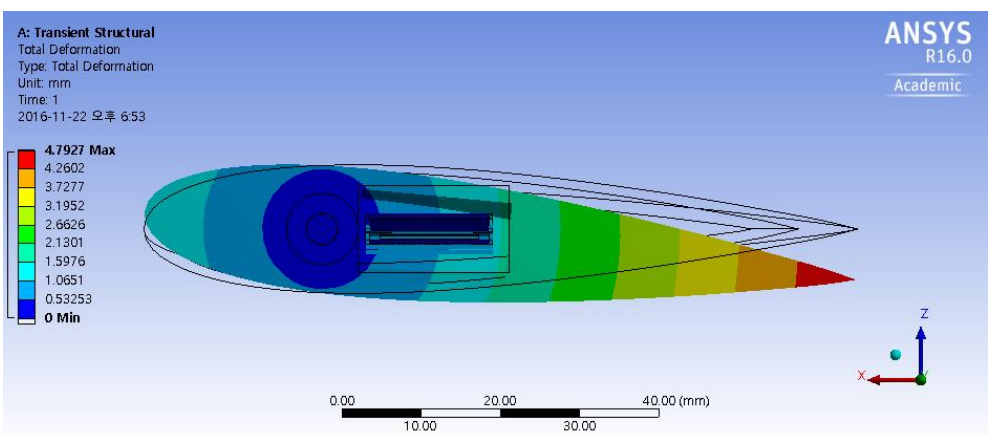

(a) Side view of Rotation Result of Design Candidate 3

(b) Isometric view of Rotation Result of Design Candidate 3

Figure 4.10 Rotation Result of Design Candidate 3 (When Presence Dummy Component Resistance)

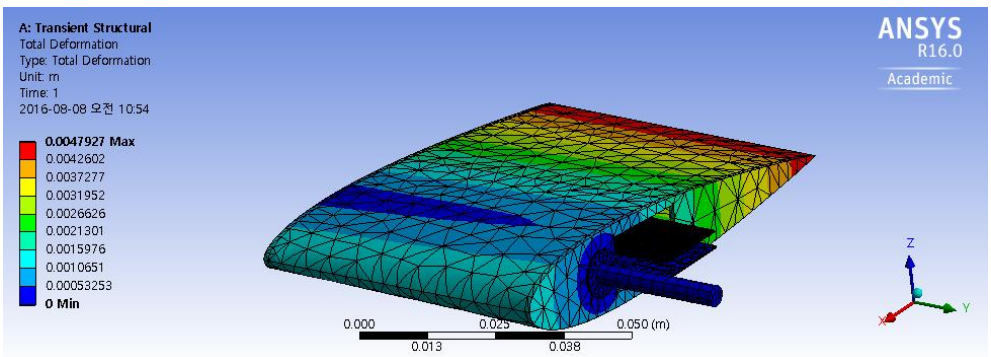

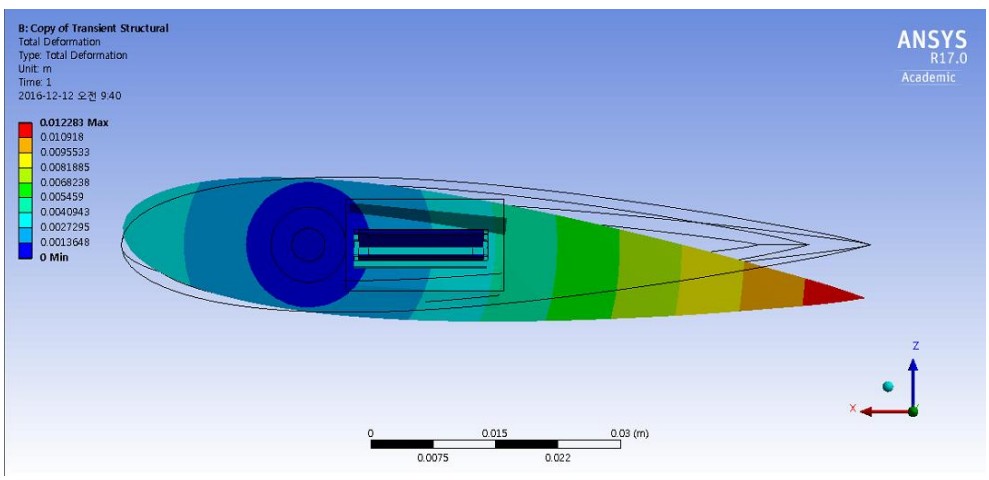

(a) Side view of Rotation Result of Design Candidate 3

(b) Isometric view of Rotation Result of Design Candidate 3

Figure 4.11 Rotation Result of Design Candidate 3 (When Dummy Component Properties Scale Down)

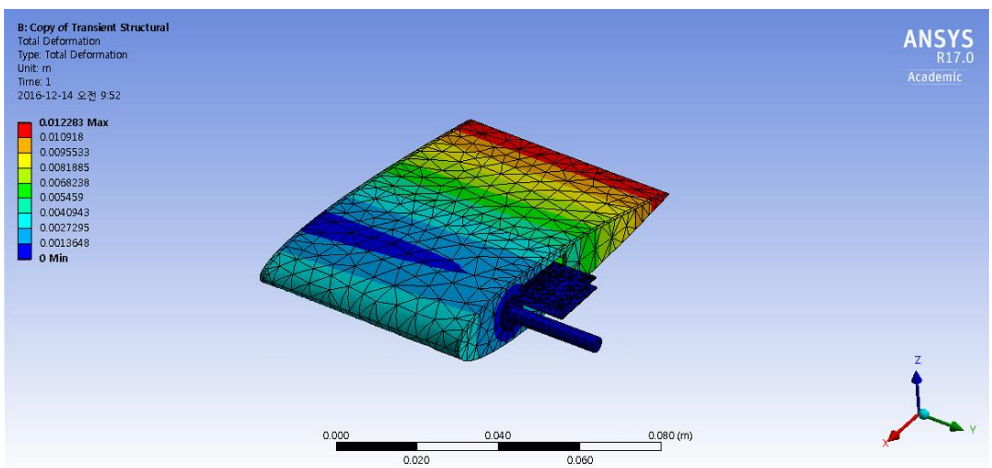

Table 4.3 Comparison of Rotation Performance of Smart Fin

	Analysis Result (ANSYS)

Design Candidate 2 (Piezoelectric Material : 3203HD)	3.71°
Design Candidate 3 (Dummy Part Resistance)	4.1° (+10.5%)
Design Candidate 3 (Dummy Par Scale Down)	10.6° (+158%)

4.3 Prediction of Rotation Pitch Angle of the Smart Fin with Aerodynamic Load

Prediction of rotation pitch angle of the smart fin when aerodynamic load is applied is conducted by using ANSYS Fluent and CFX. At first, 2-way Fluid-structure interaction (FSI) analysis is conducted regarding Design Candidate 2, and the result shows that the rotation pitch angle of the smart fin little is decreased comparing with that with no aerodynamic load when flight speed is 10m/s [21]. However, 2-way FSI analysis takes long analysis time and has convergence problem during several iterations.

Therefore, the aerodynamic hinge moment and actuator toque of the smart fin is measured to derive the rotation pitch angle of the smart fin when the aerodynamic hinge moment and actuator torque have same value regarding Design Candidate 3. In ANSYS Structural analysis, the reaction force can be calculated at the boundary condition. Therefore fixed support condition prescribes at the trailing edge of the smart fin and the reaction force is evaluated. Actuator torque is calculated by multiplying the reaction force and the length between the hinge and trailing edge. To predict the aerodynamic hinge moment of the smart fin, the moment coefficient when the angle of attack is $10°$ is derived by using ANSYS Fluent. Then, the aerodynamic hinge moment is calculated by using pitching moment equation expressed below:

$$M = C_m qSc, \quad q = \frac{1}{2}\rho v^2 \tag{23}$$

where M is pitching moment and also aerodynamic hinge moment of the smart fin, q is dynamic pressure, ρ is density of air, v is fluid velocity (m/s), S is smart fin wing area and c is chord length of the smart fin. The moment coefficient is compared when the hinge of smart fin is located at 1/5, 1/4 and 3/10 of chord line to reduce the aerodynamic hinge moment. The result shows that the moment coefficient has smallest value when hinge is located at 1/4 of chord line. Therefore, the aerodynamic hinge moment is calculated when hinge is located at its original location, 1/4 of chord line.

By deriving aerodynamic hinge moment and actuator torque of the smart fin, the moment-pitch angle diagram is plotted when flight speed is 30m/s. There is an assumption that pitch angle and moment is linearly related. Therefore, aerodynamic hinge moment linearly is increased according to pitch angle, in contrast, the actuator torque linearly is decreased. Intersecting point of the diagram is final

resulting rotation pitch angle of the smart fin when aerodynamic load is applied. The moment-pitch angle diagram when flight speed is 30m/s is plotted as shown in Fig 4. 16. In Design Candidate 3 when resistance of dummy component exists, the resulting rotation of pitch angle is decreased to be approximately 3.66°. It is almost 12.4% decrease compared with the result when aerodynamic load is not applied. In Design Candidate 3 when material properties of dummy actuator is reduced to be 1/100 of its original value, the resulting rotation of pitch angle is decreased to be approximately 8.83°. It is almost 16.7% decrease compared with the result when aerodynamic load is not applied. Those results shows that the rotation pitch angle of the smart fin is decreased as 12~16% when the aerodynamic load is applied. Therefore, the final rotation pitch angle of the smart fin is 8.83° when aerodynamic effect is considered.

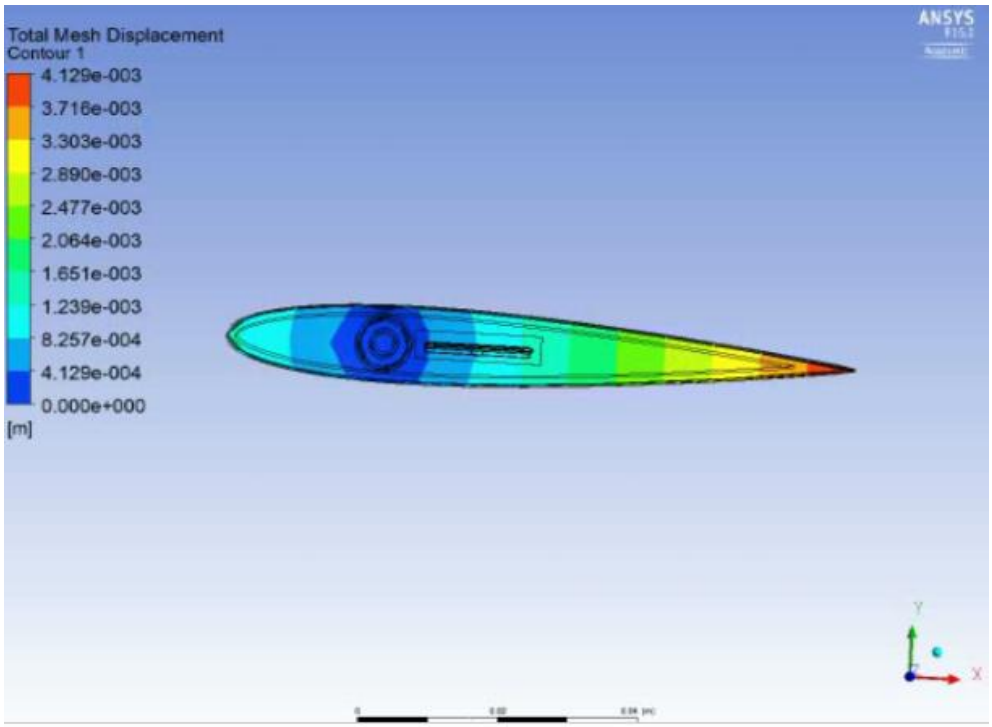

Figure. 4.12 2-way Fluid-Structure Interaction (FSI) Result of Design Candidate 2 [21]

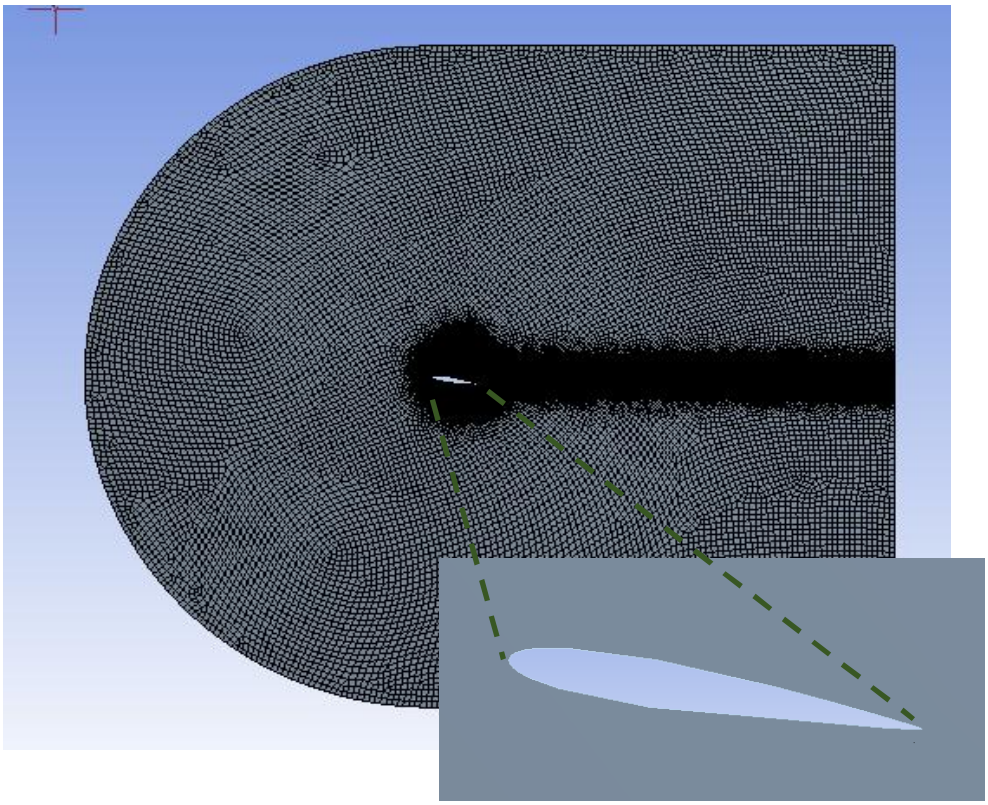

Figure 4.13 Grid Geometry of Wind Tunnel Model for ANSYS Fluent Analysis

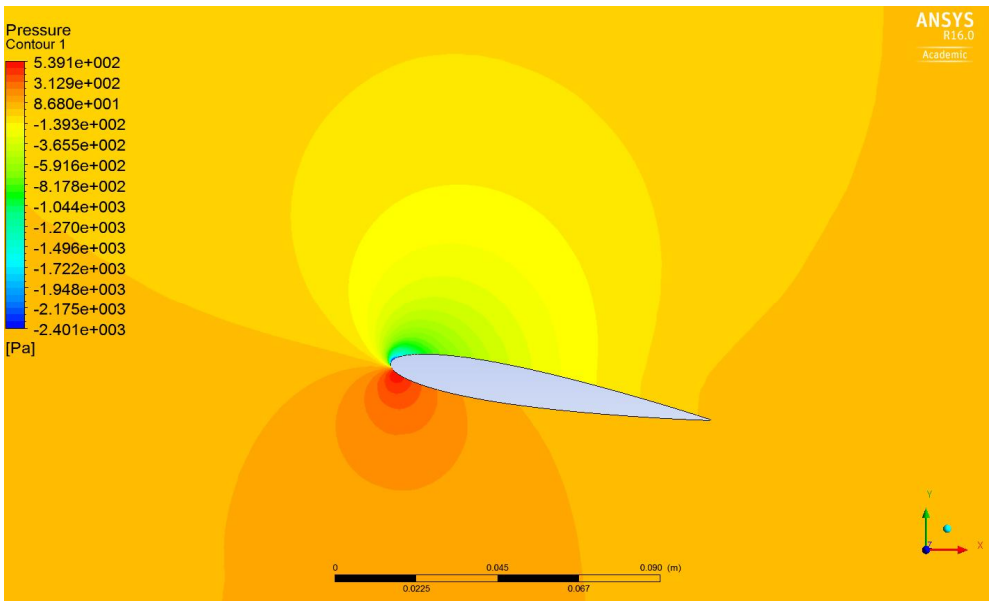

Figure 4.14 Pressure Distribution of NACA0012 When Angle of Attack is 10°

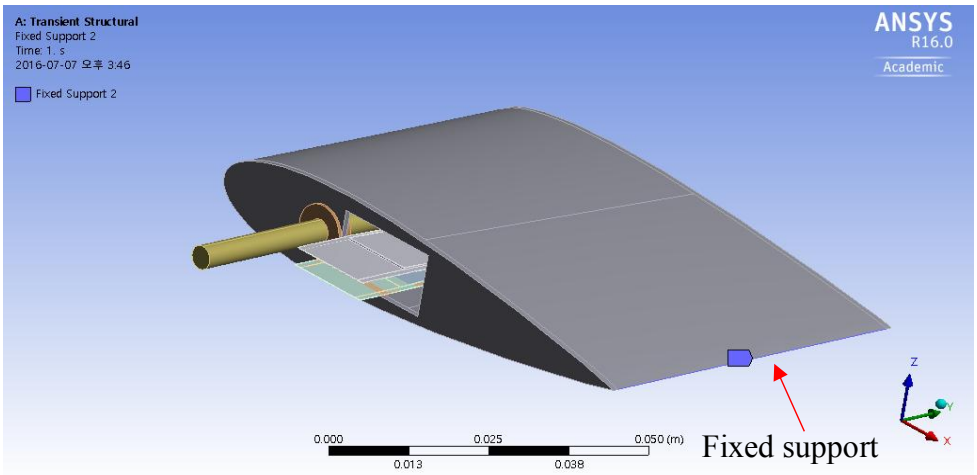

Figure 4.15 Boundary Condition for deriving Actuator Torque

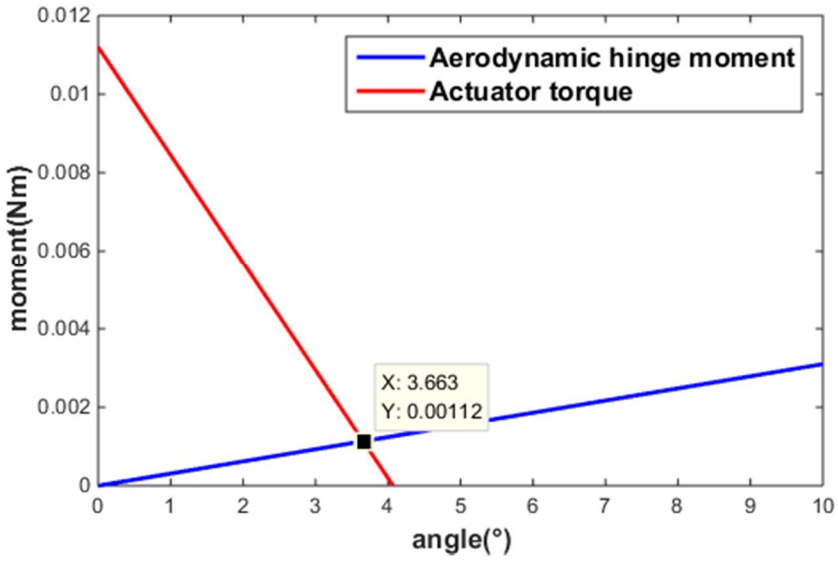

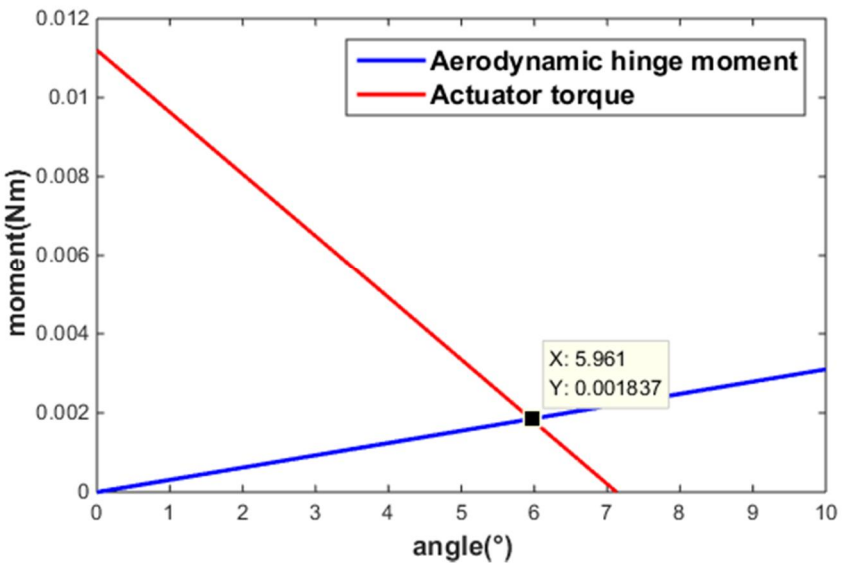

(a) Result of Pitch angle when Resistance of Dummy Component exists

(b) Result of Pitch angle when Resistance of Dummy Component reduces

Figure 4.16 Results of the Two Moments and Pitch Rotation Performance

Table 4.4 Comparison of c_m, c_l and c_m according to location of hinge at chord line

Location of hinge	c_m	c_l	c_d
1/4 of chord line	0.0116	0.884	0.0437
1/5 of chord line	0.0294	0.913	0.0314
3/10 of chord line	0.0549	0.886	0.0434

Table 4.5 Resulting Rotation Pitch Angle of the Smart Fin

	Resistance of Dummy Component exists	Resistance of Dummy Component reduces
No Aerodynamic Load	4.17°	10.6°
With Aerodynamic Load	3.66° (-12.2%)	8.83° (-16.7%)

V. Conclusion and Future Work

5.1 Conclusion

In this thesis, three design candidates of smart fin using piezoelectric material PMN-29PT and 3203HD is suggested for substituting hydraulic actuator. The performance of the piezoelectric actuator used in each design candidate is analyzed by using ANSYS Structural analysis and then compared with the experimental result to verify the analysis result of actuators. To improve the convergence of the result, equivalent bending moment is calculated and compared. After that, structural analysis regarding design candidates of the smart fin is conducted to predict the resulting pitch rotation performance by using ANSYS Structural analysis. Also, considering the aerodynamic loads, the aerodynamic hinge moment and actuator torque is estimated and the final resulting pitch rotation is predicted by using ANSYS Fluent.

Design Candidate 1 contains the unimorph and bimorph actuator. 400 volt is applied at the actuator and result shows rotation angle of 0.55° without external aerodynamic load when unimorph actuator is used. Its result shows too small angle of rotation, and thus the bimorph actuator is used to improve the performance of actuation on trailing edge. The pitch rotation angle of Design Candidate 1 is 6.31° in vacuum. However, contact problem occurs between the airfoil and actuator during actuation. Also bimorph actuator has voltage coupling problem in experiment, and loss of actuator bending force occurred during actuation in Design Candidate 1. Thus, Design Candidate 2 is suggested.

Design Candidate 2 uses the unimorph actuator using 3203HD. Compared with Design Candidate 2, additional component is used to connect between the actuator and airfoil. 400 volt is also applied at the actuator and result shows rotation pitch angle of 3.71° without aerodynamic loads. However, unsymmetrical

actuation and geometry problem proposed in Design Candidate 1 is occurred in Design Candidate 1, therefore, Design Candidate 3 is suggested.

Design Candidate 3 uses the unimorph actuator using PMN-29PT. Two actuators is applied symmetrically along spanwise direction to actuate symmetrically. Also, hollow fin is as taper shape by applying NACA0015 and NACA0012. 400 volt is also applied at the actuator and resulting pitch rotation of Design Candidate 3 is 4.17° without aerodynamic load. In Design Candidate 3, only one actuator is actuated, so other dummy actuator is acted as resistance. To reduce the resistance of dummy actuator, the additional component at the tip of the actuator is applied. When the design of the smart fin is modified, the resulting rotation of pitch angle is 10.6° increased more than two times compared with Design Candidate 2. Thus, by using these results, the final rotation pitch angle is predicted when the aerodynamic load is applied.

To predict the final rotation pitch angle of the smart fin with aerodynamic load, the aerodynamic hinge moment and actuator torque is estimated by deriving the moment coefficient and reaction force at the trailing edge. The result shows that final rotation pitch angle of the smart fin is decreased as 12.2% when the resistance of dummy component exists, and 16.4% when the resistance of dummy actuator reduces. Finally, the rotation pitch angle of the smart fin is 8.83° when aerodynamic effect is considered.

5.2 Future Work

In the future, aeroelastic analysis regarding Design Candidate 3 is needed to predict the flutter speed for stability of its design concept. Additionally, controller regarding Design Candidate 3 should be obtained to alleviate external disturbances such as gust. Time simulation of the smart fin will be conducted by using controller and specific pilot input. Final, fluid-structure interaction (FSI) analysis is needed to predict precisely about rotation pitch angle of smart fin. In this thesis, the rotation pitch angle with aerodynamic load is predicted by calculating aerodynamic hinge moment and actuator torque. Because its analysis does not reflect the experiment system, more realistic analysis such as FSI analysis is needed to predict rotation pitch angle when aerodynamic load is applied.

Reference

[1] Culshaw, B. "Smart structures—a concept or a reality?," Proceedings of the Institution of Mechanical Engineers, Part I: Journal of Systems and Control Engineering, 1992.

[2] Yoon, K. J., Yoon, B. S., “Design/Fabrication/Performance Test of UAV Actuator S-LIPCA with PMN-29PT Piezo-electric Single Crystal,” Journal of the KSAS, No. 11, 2013, pp. 985~988.

[3] Rabinovitch, O., Jack, R. V., “Smart Fins: Analytical Modeling and Basic Design Concepts,” Mechanics of Advanced Materials and Structures, 203, pp. 249-269.

[4] Barrett, R., “Aeroservoelastic DAP Missile Fin Development,” Smart Materials and Structures, Vol. 2, No. 2, 1993, pp. 55~65.

[5] Sahin, M., “Smart Structures and Their Applications on Active Vibration Control: Studies in the Department of Aerospace Engineering, METU,” Journal of Electroceramics, Vol. 20, Issue 3~4, 2008, pp. 167~174.

[6] Emery, J., “piezoelectricity,” STEM Society, 3 April 1997, pp.9-11.

[7] Bent, A.A, Hagood, N.W., and Rodgers, J.P., “Anisotropic Actuation with Piezoelectric Fiber Composites,” Journal of Intelligent Material Systems and Structures, Vo. 5, 6 May 1995, pp.338-349

[8] ANSYS INC. “Piezoelectric & MEMS exposure in ANSYS Workbench using ACT,” March 2015, pp.21-37

[9] Chopra, I., Sirohi, J., “Smart Structures Theory,” Cambridge University Press, Vol. 35, pp.327-329

[10] ANSYS INC., “Workbench – Mechanical Introduction 12.0,” Ch.4, May 5, 2009.

[11] ANSYS INC., “Introduction to Nonlinear Analysis,” Module 8, 2002

[12] Anonymous, “ANSYS Fluent Theory Guide, Release 15.0,” ANSYS Inc, Nov. 2013.

[13] Noh. I.S., “Performance Improvement of Smart Fin with Piezoelectric Actuator under High Speed Flight Condition,” Master’s thesis, Seoul National University, 2015.

[14] Barret, R., Gross, R.S., and Brozoski, F., “Missile Flight Control using Active Flexspar Actuators,” Smart Materials and Structures, Vol.5, No.2, 1996, pp.121-128.

[15] Park, C.W., Chung, C.H., Kang, Y.J., Shin, S.J., Yoon, B.S., Park, J.H., Yoon, K.J., “Structural Analysis of Smart Fins Operated by Piezoelectric Actuators for Performance Improvement,” The 26th International Conference on Adaptive Structures and Technologies, Japan, 2015

[16] Yoon, B.S., “A Study on Smart Structure for Small Missile Fin using Piezo-electric Single Crystal Actuator,” Doctoral thesis, Konkuk University, 2015

[17] Kang, Y.J, Park, C.W., Shin, S.J., Yoon, B.S., Park, J.W., Yoon, K.J., Choi, H.Y., “Design of Control Law and Aeroservoelastic Response Simulations for the All-moving Smart Fin using MATLAB/Simulink,” The 27th International Conference on Adaptive Structures and Technologies, USA, 2016

[18]Cho, J., Luo, J.J., Daniel, I.M., “Mechanical Characterization of Graphite/epoxy Nanocomposites by Multi-scale Analysis,” Composites Science and Technology, 207, 2007, pp.2399-2407

[19]Lee, H.Y., “Material Constants of (011) PMN-29PT Single Crystals [Orthorhombic:mm2],” Ceracomp, March, 20, 2012

[20] Kang, Y.J., “PI Controller Design and Aeroservoelastic Analysis of a Smart Fin Including Piezoelectric Actuator for Performance Improvement,” Master’s

thesis, Seoul National University, 2016.

[21] Park, C.W., Kang, Y.J., Shin, S.J., Yoon, B.S., Yoon, K.J., “CFD-CSD Coupled Analysis of Smart Fins Operated by Piezoelectric Actuators,” KSAS 2016 Spring Conference, Dae Myung Resort Delpino, Seorak, 2016.

국문 초록

단결정 압전재료 작동기를 이용한 강체 회전형태의 지능형 조종익 구조 설계 및 해석

박 철 우
기계항공공학부
서울대학교 대학원

기존의 유압식 작동기를 대체하기 위하여 압전재료와 같은 지능 재료로 이루어진 작동기가 연구되어 왔다. 본 논문에서는 단결정 압전 재료로 조종익 끝단을 변형시키는 설계를 바탕으로 구조해석 및 작동기 모멘트와 공력 힌지 모멘트 선도를 통한 공력이 작용할 때 최종 회전 변위각을 도출하여 풍동실험 결과와 비교하였다. 조종익은 압전 재료 작동기를 기반으로 뿌리부분은 NACA0015, 끝 부분은 NACA0012인 테이퍼 형태의 익형에 부착되어 힌지를 기준으로 강체 회전하는 형태이다. 압전재료 작동기는 작동기 내부의 압전재료에 전압 차가 적용되면 굽힘력이 유도되어 피치 모멘트를 유발하여 피치 각도를 조절할 수 있도록 설계하였다. 압전 재료 작동기가 장착된 조종익에 대한 구조 및 공력해석은 상용 프로그램인 ANSYS를 사용하여 수행하였다. 압전 구동기를 적용한 조종익을 무부하 상태에서의 변위각에 마하수 0.1 이하의 공력해석 결과를 반영한 부하상태의 최종변위각을 도출하였다. 성능 향상을 위해 조종익 내부에 압전 재료 작동기를 추가하여 구동시킨 해석결과를 제시하였으며, 내부 힌지 위치에 따른 공력 힌지 모멘트 비교 결과를 제시하여 최적의 성능을 낼 수 있는 설계 메커니즘을 제시하였다.

주요어 : 지능형 조종익, 압전재료, 지능재료 작동기 이론, ANSYS Structural Analysis, ANSYS Fluent

학 번 : 2015-20771